NASA CONTRACTOR
REPORT

NASA CR-1727
c.1

AN EXPERIMENTAL INVESTIGATION
OF THE INTERACTION OF
PLASMAS WITH ANTENNAS

by W. C. Taylor

Prepared by
STANFORD RESEARCH INSTITUTE
Menlo Park, Calif. 94025
for Langley Research Center

NATIONAL AERONAUTICS AND SPACE ADMINISTRATION • WASHINGTON, D. C. • DECEMBER 1970

1. Report No. NASA CR-1727	2. Government Accession No.	3. Recipient's Catalog No.
4. Title and Subtitle AN EXPERIMENTAL INVESTIGATION OF THE INTERACTION OF PLASMAS WITH ANTENNAS		5. Report Date December 1970
		6. Performing Organization Code
7. Author(s) W. C. Taylor		8. Performing Organization Report No. 7729
		10. Work Unit No.
9. Performing Organization Name and Address Stanford Research Institute Menlo Park California		11. Contract or Grant No. NAS 1-8889
12. Sponsoring Agency Name and Address National Aeronautics and Space Administration Washington, D.C. 20546		13. Type of Report and Period Covered Contractor Report
		14. Sponsoring Agency Code

15. Supplementary Notes

16. Abstract

A program of measurements is reported related to two phenomena of plasma/antenna interaction. The major portion of the program consisted of measurement of admittance of three antennas exposed to the plasma of the SRI 12-inch shock tube. These three antennas are part of the plasma diagnostic flight instrumentation of the Reentry Attenuation Measurements program (RAM) of NASA's Langley Research Center. Most of the measurements were made at a single pressure level (0.1 torr initial tube pressure), but over a wide range of electron density (10^{10} to 10^{13} el/cm^3). The results are compared with theoretical predictions.

In the other portion of the program, an exploratory experiment was performed to investigate techniques for measuring the effects of local injection of electrophilic chemicals. Sulfur hexafluoride was injected into the shock-tube flow upstream of both an X-band slot antenna and electrostatic wire probes. The effects of the injected chemical were measured with respect to both antenna breakdown thresholds and thermal ionization levels. The injection rates and microwave power were varied from shot to shot, and the results are compared with shots without injection.

17. Key Words (Suggested by Author(s)) Plasma-antenna interactions, electromagnetic wave propagation, shock tube measurements	18. Distribution Statement Unclassified --Unlimited--		
19. Security Classif. (of this report) Unclassified	20. Security Classif. (of this page) Unclassified	21. No. of Pages 63	22. Price* $3.00

CONTENTS

ILLUSTRATIONS

ILLUSTRATIONS (Concluded)

TABLE

SYMBOLS

A	Specific attenuation
b	Normalized susceptance
d	Distance from aperture (see Fig. 18)
d_c	Distance out to n_c (see Fig. 18)
D	Diffusion coefficient
f	Microwave frequency
g	Normalized conductance
i_p	Electrostatic-probe current
n	Electron density
n_c	Critical electron density
n_o	Initial electron density
n_{pk}	Peak electron density (see Fig. 18)
p_1	Initial shock-tube pressure
S	Thermal ionization source rate
t	Time
T_{eq}	Equilibrium temperature
u_s	Shock speed
V_i	Microwave voltage corresponding to incident wave
V_p	Microwave-probe voltage
α	Recombination coefficient
$|\Gamma|$	Magnitude of reflection coefficient
δ_{pk}	Distance to n_{pk} (see Fig. 18)
Λ	Characteristic diffusion length
ν	Collision frequency
ν_a	Attachment frequency

ν_i Ionization frequency

ω Microwave radian frequency

ω_p Plasma radian frequency

τ Time from beginning of pulse to time at which n reaches n_c

AN EXPERIMENTAL INVESTIGATION OF THE INTERACTION
OF PLASMAS WITH ANTENNAS

By W. C. Taylor
Stanford Research Institute[*]

I   INTRODUCTION

This is the Final Report on a one-year study that is the fourth in
a series, all dealing generally with the problem of communications during
hypersonic flight. The first three studies were reported earlier.[1-3][†]

The primary emphasis of this study was to determine the accuracy of
inferring electron density from measurements of the admittance of three
different antennas used on the RAM flight-test program. In addition,
preliminary measurements were made to study the effects of local addition
of sulfur hexafluoride to the hypersonic flow, with respect to both an-
tenna breakdown thresholds and thermal ionization levels.

Section II of this report concerns the admittance measurements, and
Section III is a discussion of the use of measured antenna admittance
to infer the flight-test plasma properties, especially the profile of
the electron density normal to the vehicle surface. Section IV reports
the measurements with sulfur hexafluoride injection.

---

[*] Senior Research Engineer, Stanford Research Institute, Menlo Park,
     California.
[†] References are listed at the end of the report.

1

II ADMITTANCE MEASUREMENTS

Two of the antennas tested in this program have already been tested on RAM flight tests (RAM C antennas) and one will be flown in a future flight test (RAM C-C). The SRI arc-driven 12-inch shock tube can be used to produce plasmas that are similar in both gas density and inboard boundary-layer profile of electron density found around blunt bodies in the altitude range between about 75 and 175 kft. The tests reported here at 0.1 torr initial pressure give conditions similar to those near the upper end of this flight range. It was the purpose of these measurements to determine how close to theory the antennas operate in a single regime pertinent to the RAM flights.

A. Description of Antennas and Shock-Tube Mounting

The SRI arc-driven 12-inch shock tube is described in Ref. 3. For the measurements reported here, it was desirable to mount the antennas in the tube such that the reflective metal shock-tube wall was not directly opposite the antennas. For this reason, an auxiliary fiberglass tube 10-inches in diameter (inside) was designed and fabricated to essentially extend the tube test section into the existing 36-inch-diameter dump tank. This auxiliary tube is shown in Figure 1, showing two antennas mounted on a curved ground plane and attached at the downstream end of the fiberglass tube. The sharp leading edge of the fiberglass tube was located upstream of the dump tank, such that the tube served as a channel for most of the test slug to flow unexpanded into the dump-tank area where the antennas were located. Figure 2 shows the sharp leading edge of the Teflon coating on the curved ground plane, fashioned to allow the test slug of hot air to pass essentially undisturbed between the Teflon

SHOCK-TUBE
FLOW DIRECTION

GROUND PLANE

FIGURE 1   FIBERGLASS TUBE WITH RAM C ANTENNAS MOUNTED AT DOWNSTREAM END

TA-7729-27

TA-7729-4
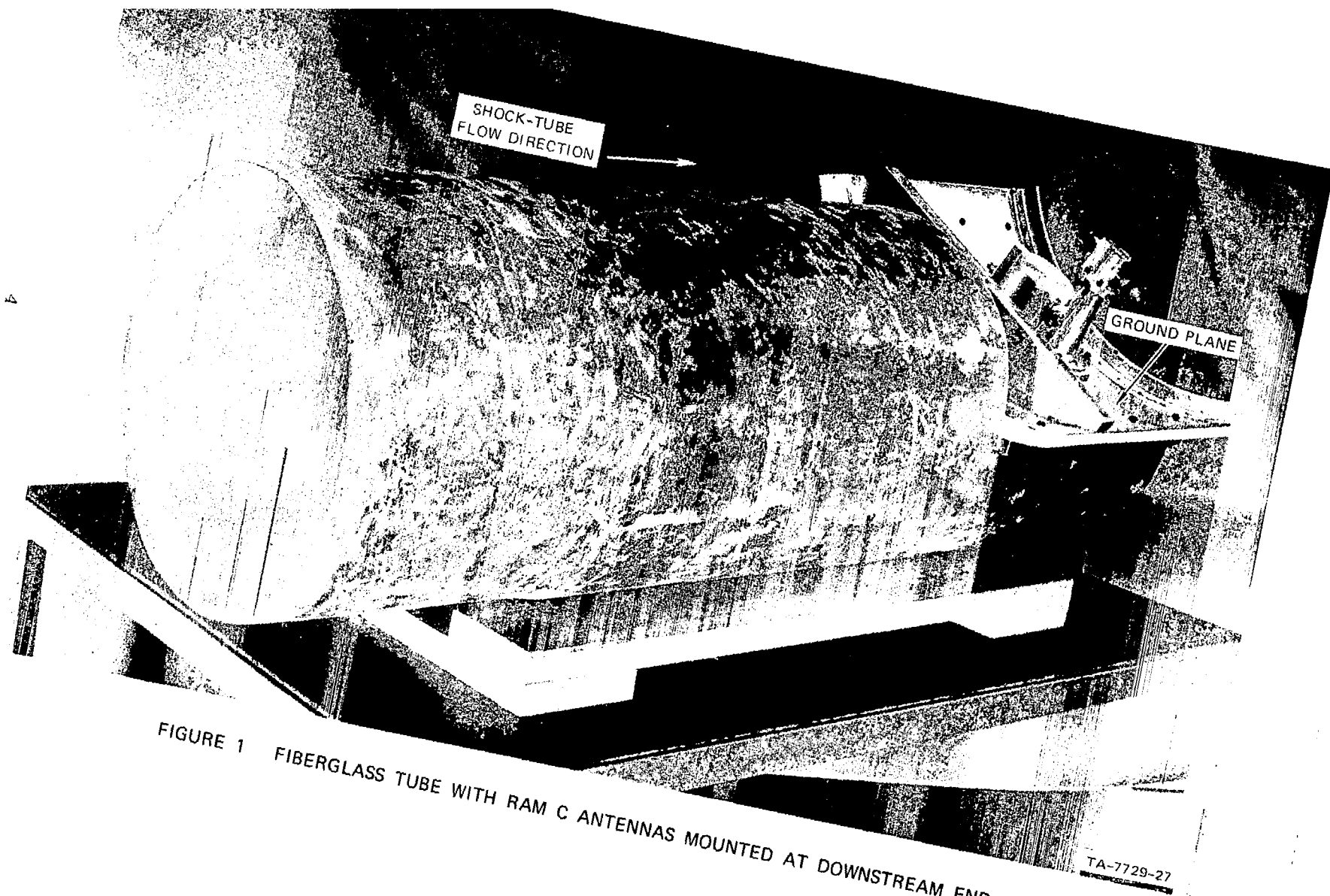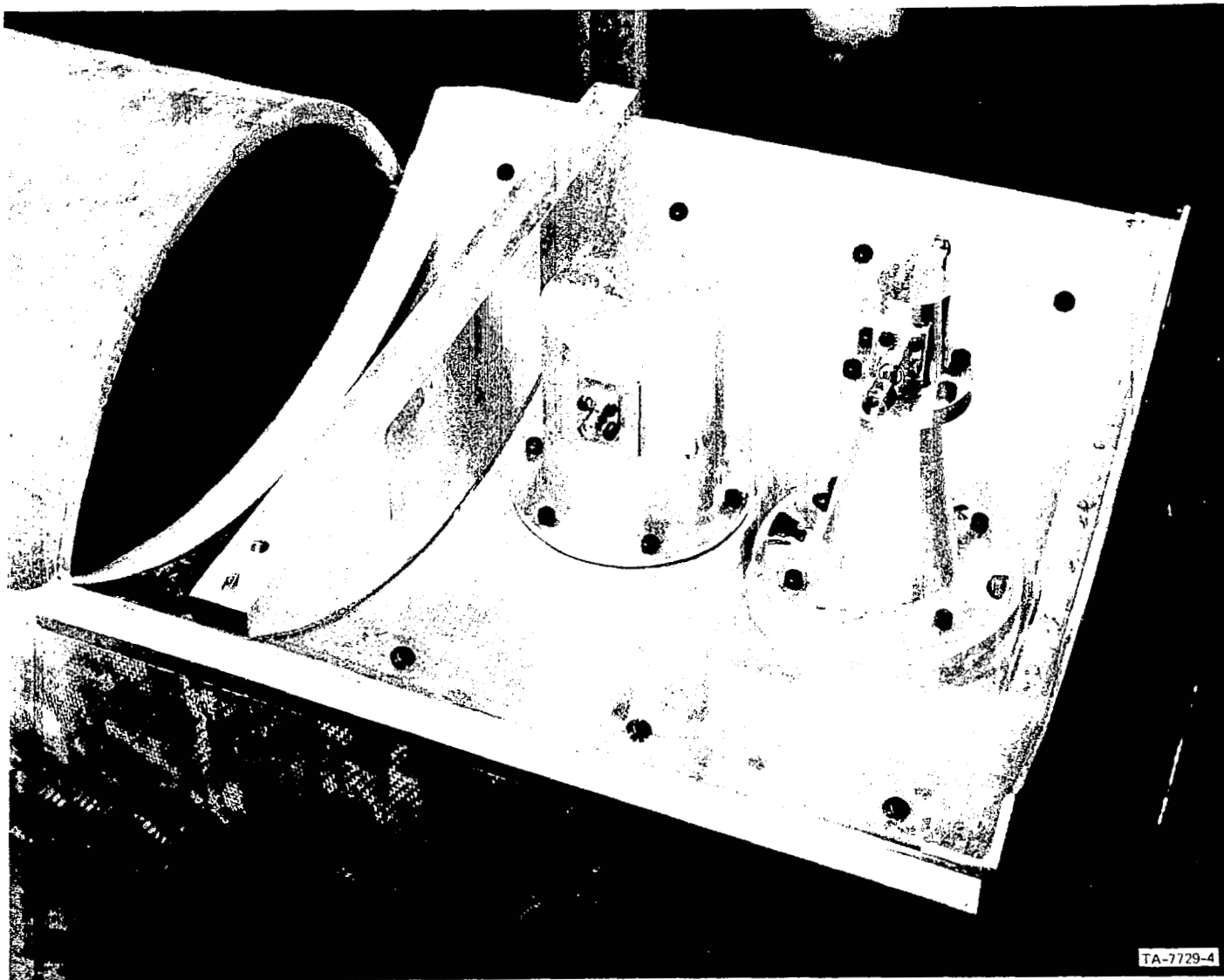
FIGURE 2   RAM C ANTENNAS MOUNTED ON GROUND PLANE

layer and the fiberglass. Figure 3 shows the side of the ground plane over which the test plasma passed. The test plasma over the ground plane was about six inches deep and ten inches wide. Also shown is the window that was cut in the fiberglass to reduce the reflection coefficient without plasma to a minimum level. This window was covered by thin Mylar on the inside surface to preserve the surface continuity. Microwave absorber was placed between the fiberglass and the dump tank to isolate the metal tank walls from the antennas. Before the antennas were mounted on it, the fiberglass tube was inserted in the shock tube for some 0.1-torr test shots. A rake of wire probes across the downstream end of the tube showed that the fiberglass did not measurably affect the electron density in the test slug at this pressure.

Figure 3 also shows the array of six 10-mil-diameter wire probes used to map the test-plasma electron density for the low-pressure shots. For the high-pressure shots, two wedge probes were placed just downstream of the apertures at distances of 1/8-inch and 7/8-inch off the Teflon layer. Both types of probes were described in Ref. 3.

On the basis of measurements reported earlier,[4] estimates can be made of the electron-density boundary-layer thickness. In terms of the distance δ from the Teflon surface out to the half-peak-density point, the results are: for the S-band antennas, δ = 2 mm at 0.1 torr and 0.7 mm at 1 torr; further downstream, for the X-band antenna, δ = 2.5 mm at 0.1 torr and 0.9 mm at 1 torr.

Figure 2 shows the two RAM C antennas designed for use as reflectometers on RAM flight tests. The main purpose of these antennas was to indicate, by a precipitous change in reflection coefficient, the time at which the plasma density went through a small range of electron density near the critical value. The antenna on the left in Figure 2 is the S-band one, radiating at 3348 MHz, and on the right is the X-band one,
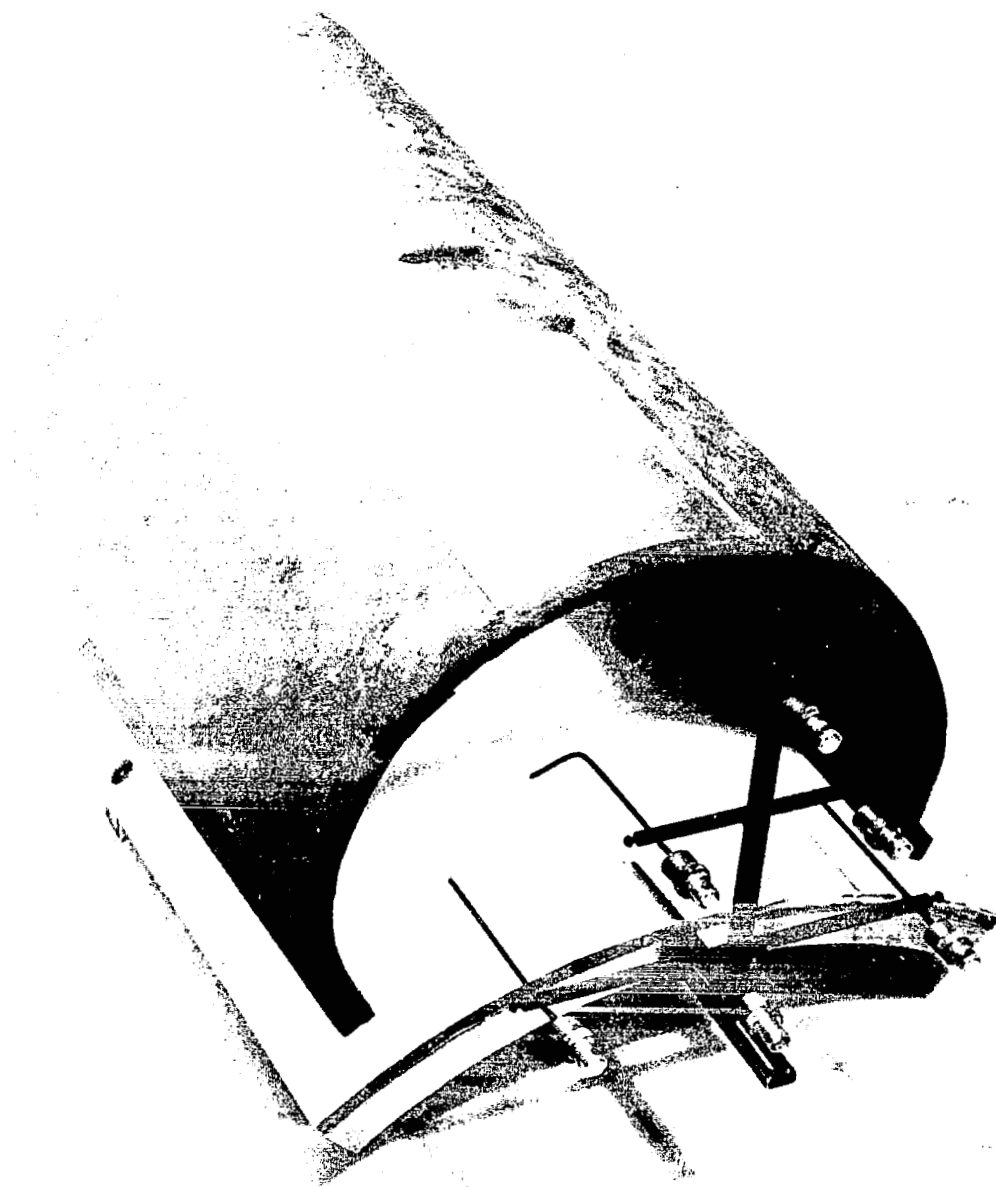
FIGURE 3   VIEW OF TEST FACILITY INCLUDING ELECTROSTATIC PROBE ARRAY
AND WINDOW IN FIBERGLASS (antenna aperture covered by Teflon layer)

at a frequency of 10.044 GHz. Both have tuning screws for providing a free-space match. The metal conducting walls of both antennas were extended through the Teflon coating to achieve the greatest possible proximity to the plasma.

Measurements were also conducted of the admittance of the S-band diagnostic RAM C-C antenna. This antenna, also circular, was designed to provide a calculable scattering matrix so that the plasma conditions over the aperture could be related to the measured terminal admittance over a wide range of electron density.

Block diagrams of the microwave circuitry used to measure the rapidly changing admittance of the antennas are shown in Figure 4 (S-band) and Figure 5 (X-band). The main feature of the S-band system is the slotted line with three microwave probes used to detect the local electric-field standing wave. If the incident power is determined by other means, only two probes are needed to determine admittance, but a third probe at a still different electrical location in the line improves the precision of the measurement. (During early measurements, the S-band system consisted of two probes and a reflected directional coupler, but the three-probe method was found to be more accurate when coaxial equipment is used.) The tuners were needed to cancel out the susceptance introduced by the couplings in the somewhat complicated transmission lines between the microwave instrumentation external to the dump tank and the antenna terminals in the approximate center of the tank. The X-band system also included a directional coupler to monitor the incident level, similar to that shown for the S-band system.

It had been found earlier[3] that in the low-pressure shots the use of a liquid-nitrogen trap in the shock tube to remove the water vapor from the test air served to increase the length of the nominally uniform test plasma between the shock front and the driver gases. This procedure
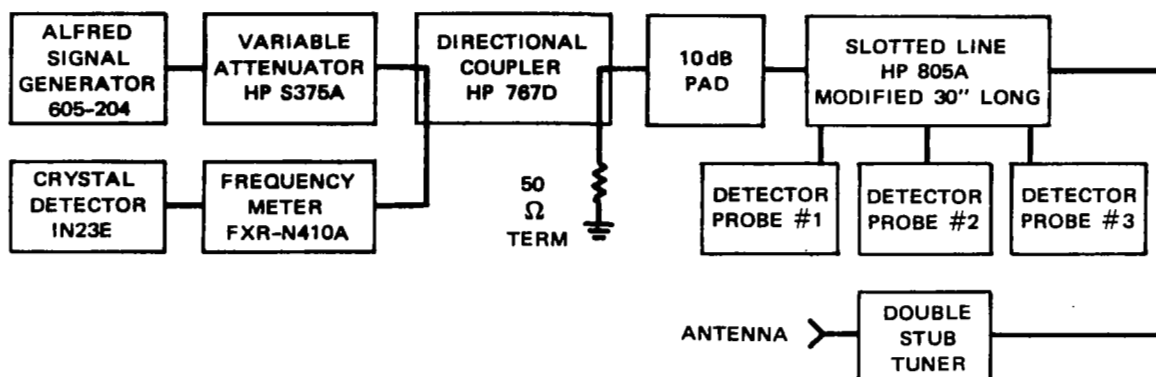
FIGURE 4 BLOCK DIAGRAM OF S-BAND EQUIPMENT FOR ADMITTANCE MEASUREMENTS
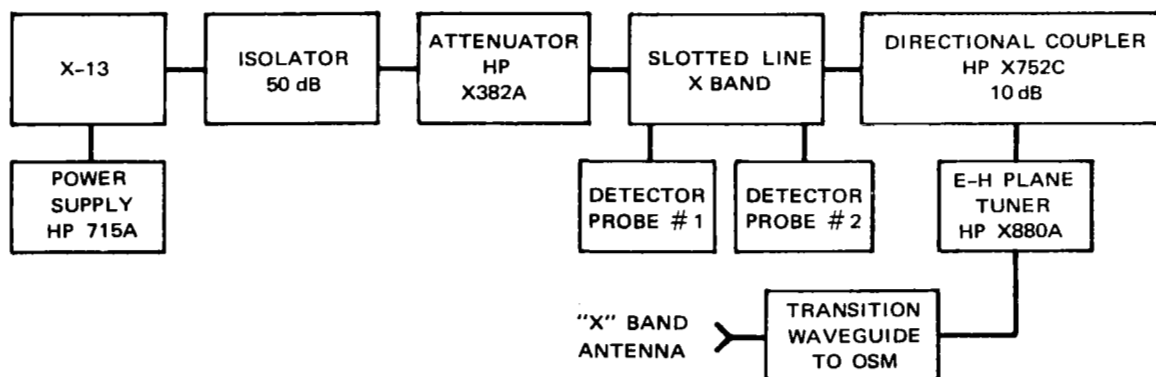
FIGURE 5 BLOCK DIAGRAM OF X-BAND EQUIPMENT FOR ADMITTANCE MEASUREMENTS

was used in these tests especially since the larger aperture sizes
($\sim$3 inches) presented a more stringent requirement for test-plasma length
than in the previous work.[3] It was initially planned that only 0.1-torr
measurements would be made, but some 1.0-torr shots were fired toward the
end of the program.

It was found early in the admittance tests that, although liquid
nitrogen was being used for a water-vapor trap to improve the quality
and duration of the test period, there was a high incidence of poor-
quality test plasmas as evidenced by very short test times on some of
the probes. Many test shots were run to isolate the source of the
trouble, and it turned out that almost all the shots when the microwave
absorber was not in the tube gave very good test slugs. As a result,
the absorber was placed in a Mylar vacuum enclosure of its own to isolate
it from the test air. The subsequent results were consistently good. It
is assumed that outgassed impurities from the absorber in the test air
caused the problem, but it is not understood how. The absorber used
was Eccosorb AN-75.

B. Results of Measurements on RAM C Antennas

1. Preliminary Tests and Calibrations

The RAM C S-band antenna installed on the segment of cylindrical
ground plane was found to have a VSWR of 1.12 when radiating into free
space, while the X-band VSWR was 1.06. But when the ground plane was
mounted on the fiberglass auxiliary tube, the S-band VSWR was found to
be greater than 1.3. Solutions were sought until the window shown in
Figure 3 was cut out, giving a VSWR no greater than 1.1 for both antennas.
This was maintained when the apparatus was installed in the shock tube,
provided microwave absorber was used between the fiberglass and the metal
dump-tank wall.

In each case, measurements were made of the phase shift between the aperture (covered with a short circuit made with metal foil) and shorted terminals of the antenna so that the measured terminal admittance could be transformed to aperture admittance if it was assumed that only a phase rotation was needed to do so. For the S-band antenna, the nulls with the aperture shorted were located 0.121 guide wavelengths toward the load from the nulls with the terminals shorted. In the X-band system, the nulls with the aperture shorted were located 0.107 guide wavelengths toward the generator from the nulls with the terminals shorted.

The losses in the transmission lines between the slotted line and the antenna terminals were measured and taken into account in both cases. The use of RG-9/U coaxial cable kept the S-band one-way loss to 1.1 dB. The use of the 10-dB directional coupler in the X-band circuit between the slotted line and the antenna contributed to the total effective X-band line loss of 1.3 dB (one-way).

The X-band detector monitoring reflected signal was calibrated by putting a short at the antenna terminals and setting the attenuator at various appropriate levels. The detector levels were recorded on photographs, using the same Polaroid camera for a given detector that was subsequently used to record the shot data from this detector.

The slotted-line detectors were calibrated using a matched load to achieve a flat line. When the load admittance varies arbitrarily over the complete range from 0 to ∞, it is possible that the voltage detected by a probe in a slotted line, V_p, varies from 0 to 2 V_i, where V_i is the voltage corresponding to the incident wave alone. However, with some line losses and plasma density varying over a finite range, it was known from earlier experience that the voltage excursions could be expected to be almost always in the range of 0.4 V_i to 1.6 V_i. After setting the incident power at a known level, the calibration levels were recorded

photographically, varying the attenuator levels both higher and lower than the attenuator setting that was used for the shots. This latter setting, usually 4 dB, corresponded in the calibration levels to V_i. Figure 6, showing an example of the calibration levels, illustrates the precision available in these measurements. Since V_i corresponds to the radius of a Smith chart when the admittance is inferred from the probe levels, a Smith-chart radius is equivalent to approximately a 3-cm scale on the oscilloscope face. This could be improved, for example, by the use of single-trace oscilloscopes rather than the dual ones. However, as many as 12 channels were needed (six ion probes, three S-band, and three X-band) on some of the shots in addition to any auxiliary measurements such as shock-speed monitoring. Indeed, in some cases, M-type multiple-trace heads were used to minimize the number of oscilloscopes needed.

$$V_p / V_i$$

1.59

1.0

5.0

TA-7729-17
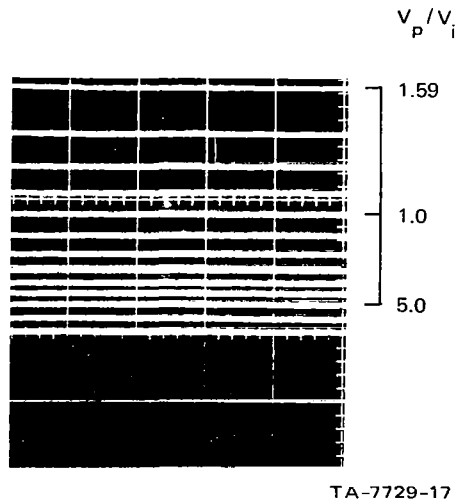
FIGURE 6   EXAMPLE OF SLOTTED-
LINE MICROWAVE-PROBE-
DETECTOR CALIBRATION
LEVELS

2. 0.1-Torr Measurement Results

Figure 7 shows the pertinent data collected on a 0.1-torr shot. For this shot, the three S-band probes were placed at eighth-wavelength intervals, with the center one (No. 2) at a point corresponding to the terminal's position. The two X-band probes were placed three-sixteenths and one-eighth wavelength, respectively, from the equivalent terminals position. Since all traces shown were triggered simultaneously, the shock arrived at the S-band aperture first, then at the X-band aperture, and then at the ion probes. The X-band aperture and probes were centered approximately 85 and 125 mm, respectively, downstream from the S-band centerline. It is seen that the ion probes are generally consistent with each other in this shot for at least the first 80 μs following the front, with the exception of a short burst on ion probe No. 5. (Ion probe No. 1, shown at the top of Figure 3, was not monitored on this shot, and ion probe No. 2 current is not shown in Figure 7.) Although the admittance generally seemed most strongly related to the electron density inferred from No. 4 (the center probe just over surface), the data was not used unless it could be seen that at least three other probes showed essentially the same density. The inferred electron density on this shot ranged from 3.2×10^{11} (just after the front) to 1.7×10^{12} (where the ion probe traces go off scale).

Since it was found that both antennas respond largely only to the plasma over the central 1.5-inch core of the aperture, corresponding to a flow time of about 10 μs, the gradient in electron density over the aperture for the 80-μs test time was no greater than approximately 20 percent. Thus, this and similar shots with a slow axial variation in electron density yielded essentially a continuum of data over this range. For data reduction and plotting, discrete points were taken at approximately 10-μs intervals. It is seen that the precipitous jumps in the X-band probe voltages and reflection coefficient (at approximately

13

$V_p/V_i = 1$ → X-BAND PROBE NO. 1

$V_p/V_i = 1$ → X-BAND PROBE NO. 2

t_1 SHOCK FRONT ARRIVES OVER S-BAND APERTURE

t_2 SHOCK FRONT ARRIVES OVER X-BAND APERTURE

t_3 SHOCK FRONT ARRIVES AT PROBES

0.79

$|\Gamma|$

0

X-BAND REFLECTION COEFFICIENT

ION PROBE NO. 3

$V_p/V_i = 1$ → S-BAND PROBE NO. 1

$V_p/V_i = 1$ → S-BAND PROBE NO. 2

$V_p/V_i = 1$ → S-BAND PROBE NO. 3

ION PROBE NO. 4

ION PROBE NO. 5

ION PROBE NO. 6

50μs

TIME →
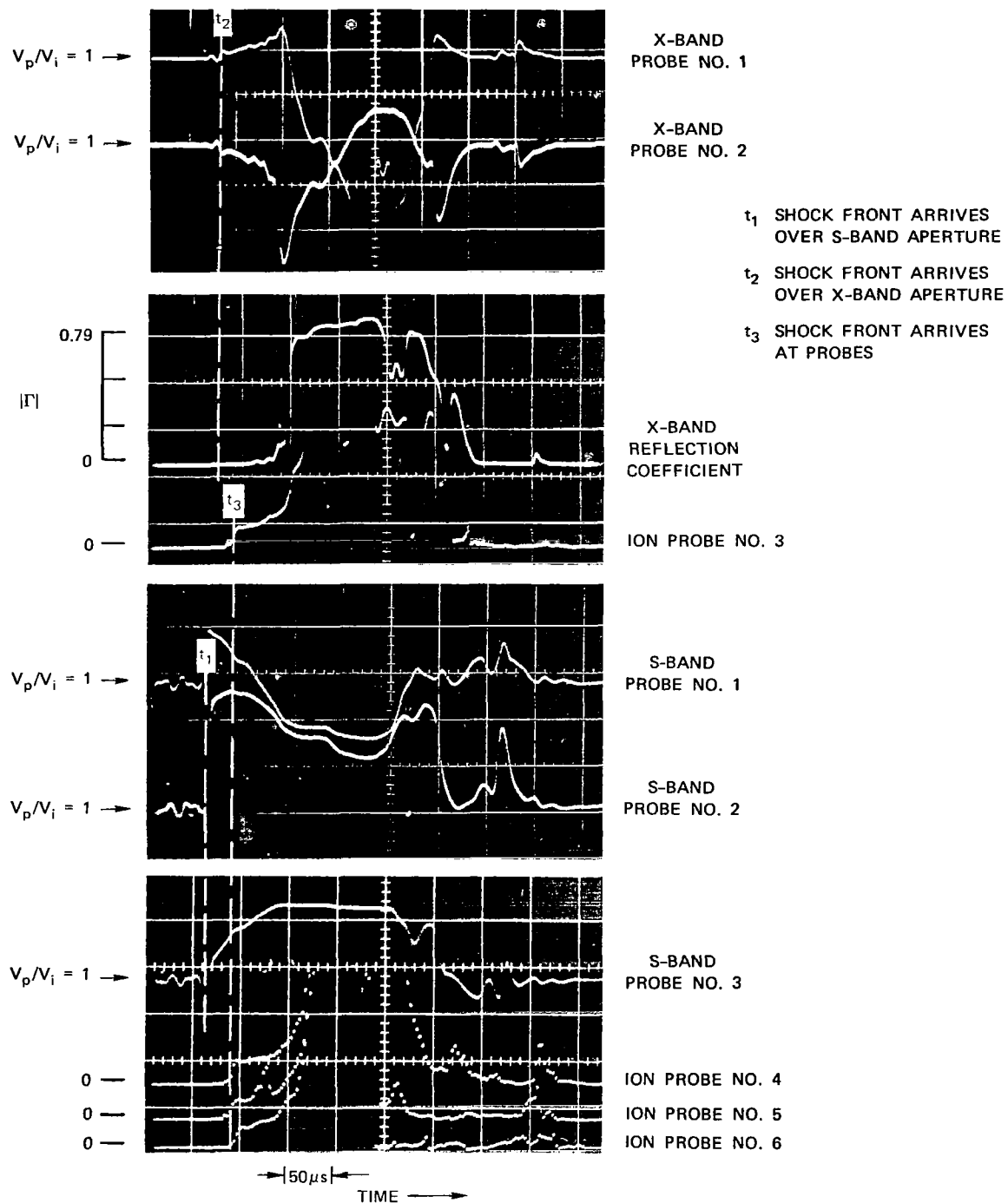
TA-7729-18

FIGURE 7   EXAMPLE OF 0.1-torr SHOT DATA ON RAM C ANTENNAS

14

65 μs following the front) occurs while the electron density and the S-band probe voltages are changing relatively gradually. The biggest jump in the S-band data occurs at the arrival of the shock front because the density just behind the front is over critical for this frequency. Note that the S-band probes respond to the front in a "rise time" of about 10 μs. It appears from the microwave data on this shot that the electron density kept increasing for a total of about 175 μs starting at the front, but the ion probe currents went off-scale such that neither density nor uniformity of the plasma is known after about 80 μs.

The composite S-band aperture admittance data are shown in Figure 8. The "ticked" circles are from the data on Figure 7. The data from the three microwave probes were converted to radii of arcs plotted on the Smith Chart from the appropriate electrical points around the perimeter. The size of a given admittance data "point" is an indication of how far the three arcs missed intersecting at a single point. The phase rotation with increasing electron density is counterclockwise, as indicated by the approximate-electron-density indicators around the periphery of the chart. The voltage-reflection-coefficient values corresponding to these data, but corrected for line loss, are plotted in Figure 9 as a function of electron density. The data from Figure 7 are indicated, with a line drawn connecting the points, since a continuum of values is available from the shot. Because such shots are so fruitful, only a few are needed to adequately indicate the admittance as a function of time. The data from other, similar shots are also represented in Figure 9 by lines inter-connecting the points.

Figure 10 shows the X-band aperture admittance data, with the points from Figure 7 identified by tick marks. Figure 11 shows the correspond-ing voltage-reflection-coefficient values versus electron density, com-pared with calculations by W. F. Croswell[*] for a somewhat smaller circular aperture. It is seen that the measurements fall within a factor of two

[*] Contract Monitor for this project.

15

$n \approx 10^{11}$

$n \approx 3 \times 10^{11}$

$n \approx 10^{12}$

$n \approx 10^{13}$

$n = 0$
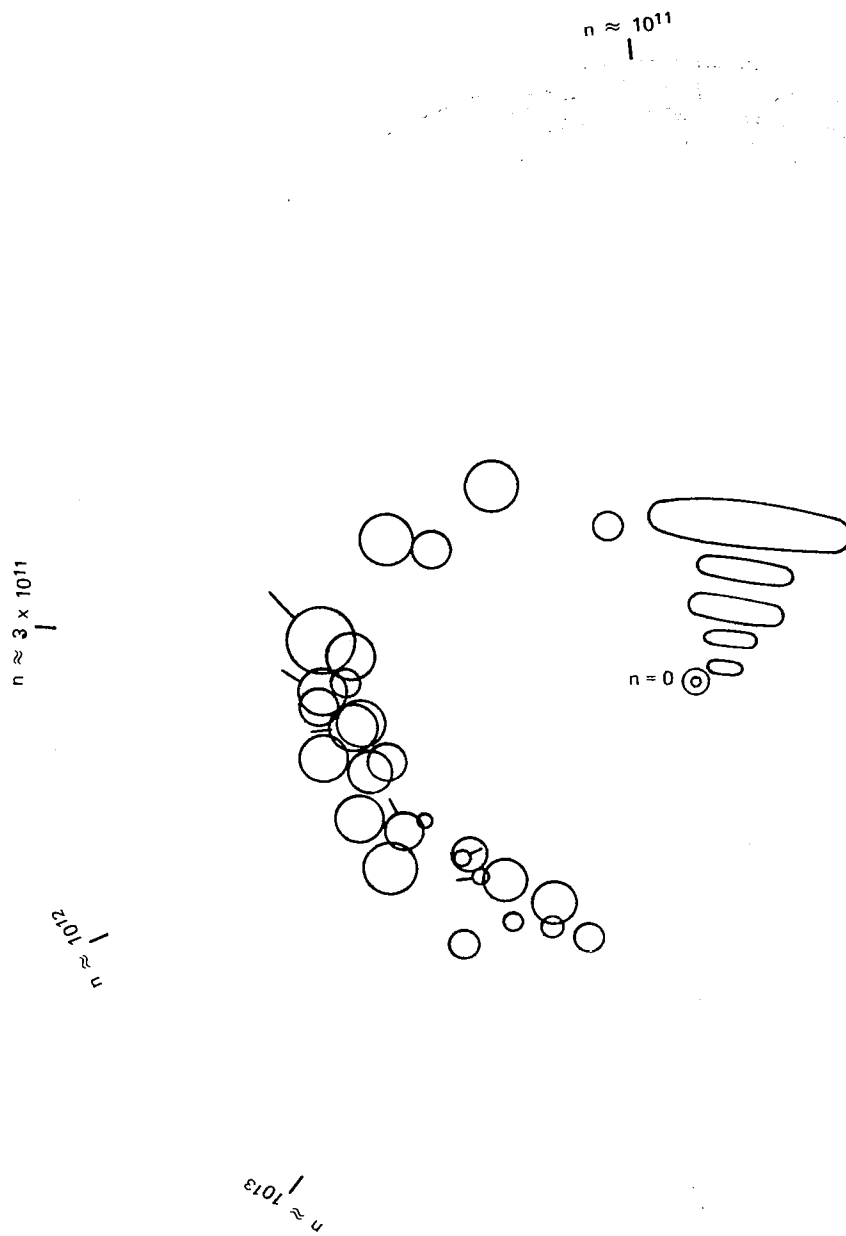
TB-7729-8R

FIGURE 8   RAM C S-BAND ADMITTANCE DATA REFERENCED TO APERTURE
(not corrected for line loss)—0.1 torr

16

1.0

0.9

0.8

0.7

0.6

|Γ| 0.5

0.4

0.3

0.2

0.1

0.0

10^{10} 10^{11} 10^{12} 10^{13} 10^{14}

n_c

DATA
FROM
FIGURE 7

n — el/cm^3

TB-7729-9R

17
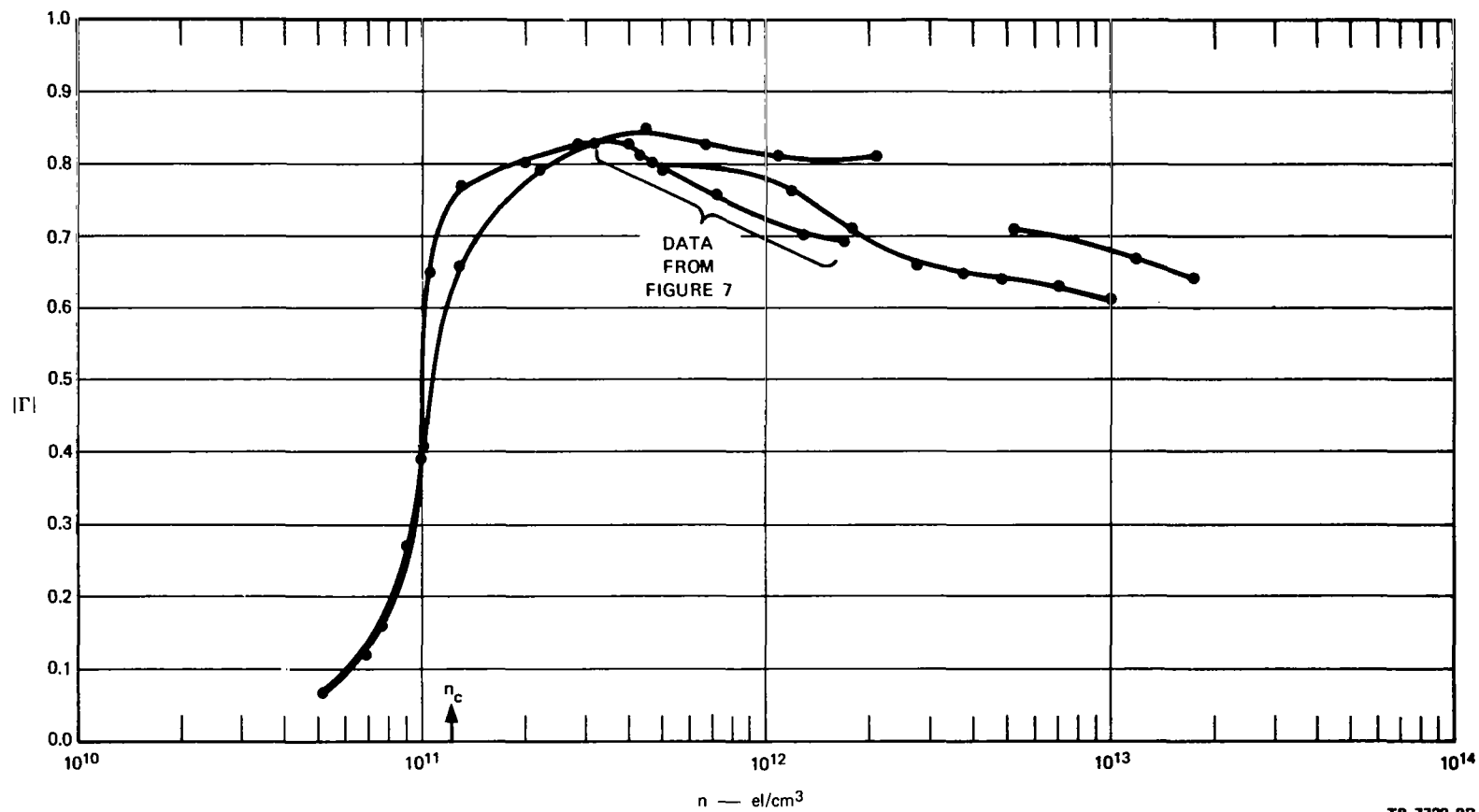
FIGURE 9   RAM C S-BAND REFLECTION COEFFICIENT AS A FUNCTION OF ELECTRON DENSITY—0.1 torr

$n \approx 10^{12}$

$n \approx 3 \times 10^{12}$

$n \approx 10^{13}$

$n = 0$
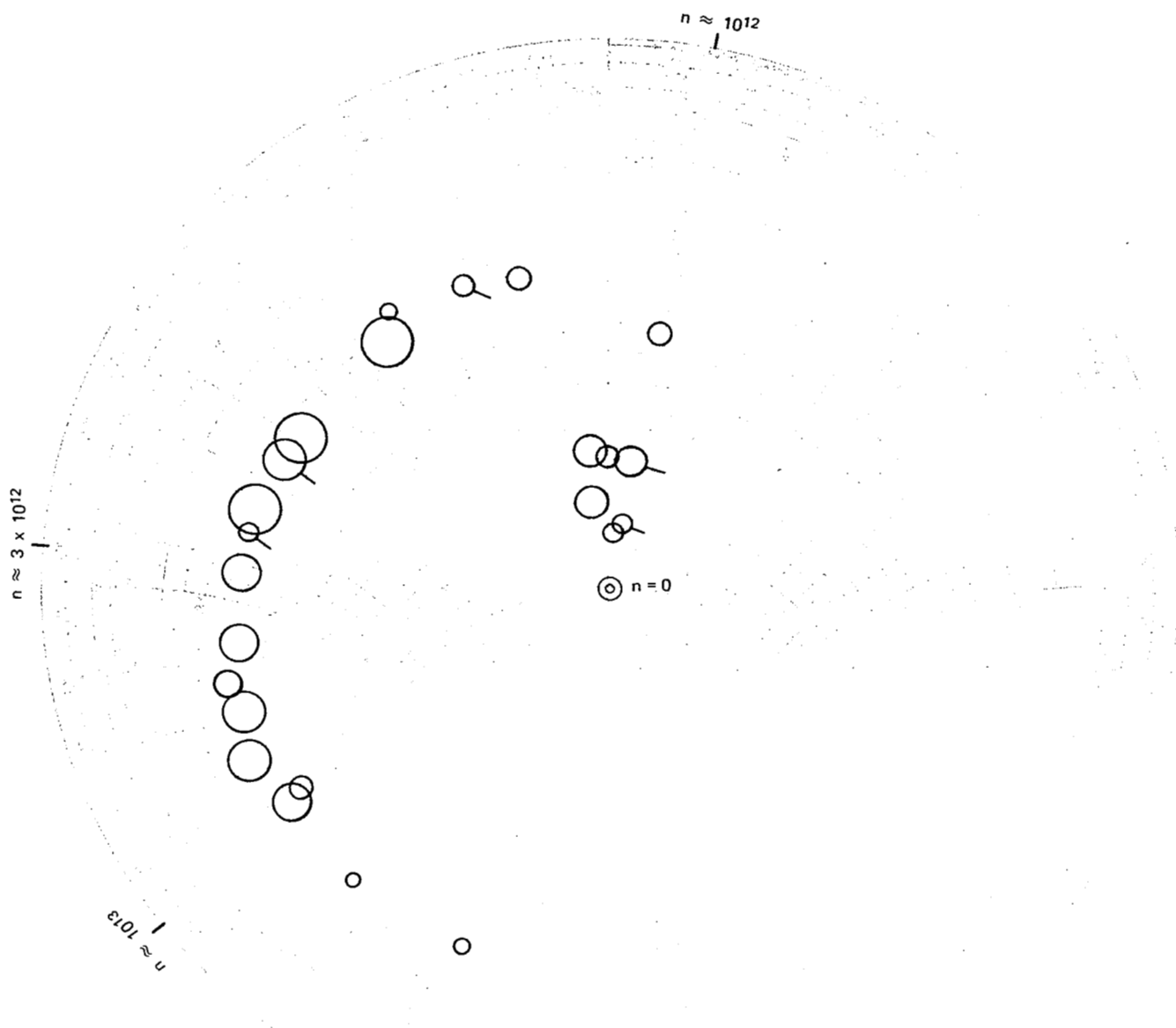
TB–7729–6R

FIGURE 10 RAM C X-BAND APERTURE ADMITTANCE (line-loss corrected)—0.1 torr
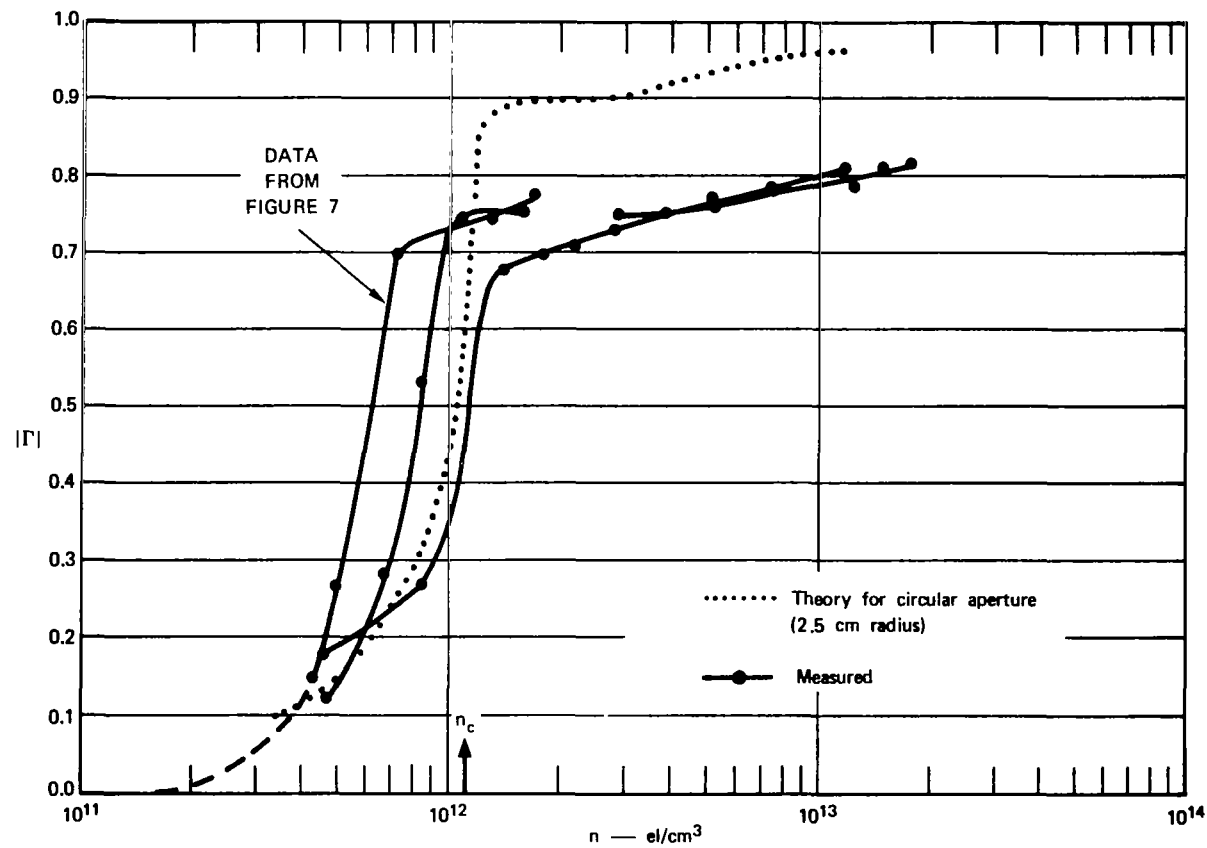
TB-7729-7R

FIGURE 11   RAM C X-BAND REFLECTION COEFFICIENT AS A FUNCTION OF ELECTRON
DENSITY, MEASURED AND THEORY—0.1 torr

of the theory up to $|\Gamma| = 0.7$, and that the slope of the curves from single shots agrees quite well with the theory. Since the maximum slope is largely determined by collision frequency, the agreement in slope is an indication that the collision frequency was close to the value calculated from the shock speed and pressure--2.5×10^9.

The admittance data of Figure 10 were plotted in Figure 12 as a function of n, and compared with theoretical aperture admittance calculated by Croswell. (The electron density corresponding to the two points well above 10^{13} if Figure 10 is not known.) It is seen that the conductance values agree well only up to critical, as does the reflection coefficient in Figure 11. It is possible that above critical the discrepancy in both conductance and reflection coefficient is due to the fact that the theory applies to an antenna terminating in a conducting ground plane, whereas the RAM C antennas terminate at the surface of the Teflon. It is possible that a larger conductance arises because the energy can be radiated through the Teflon off to the side of the ground plane, rather than being confined to the narrow layer of undercritical plasma next to the surface. The susceptance data agree quite well with the theory except for translation in electron density for the various shot groupings. Since the ion-probe determination of electron density may be uncertain by as much as a factor of two, it is expected that the theory for susceptance is applicable to this antenna.

Thus it appears that the RAM C antennas not only accomplished the purpose of indicating by a sharp change in reflection coefficient when the electron density passed through the narrow range near critical, but in addition the phase information from the X-band antenna appears valuable in determining either electron density or profile data (see Sec. III) in a larger range above the critical density.
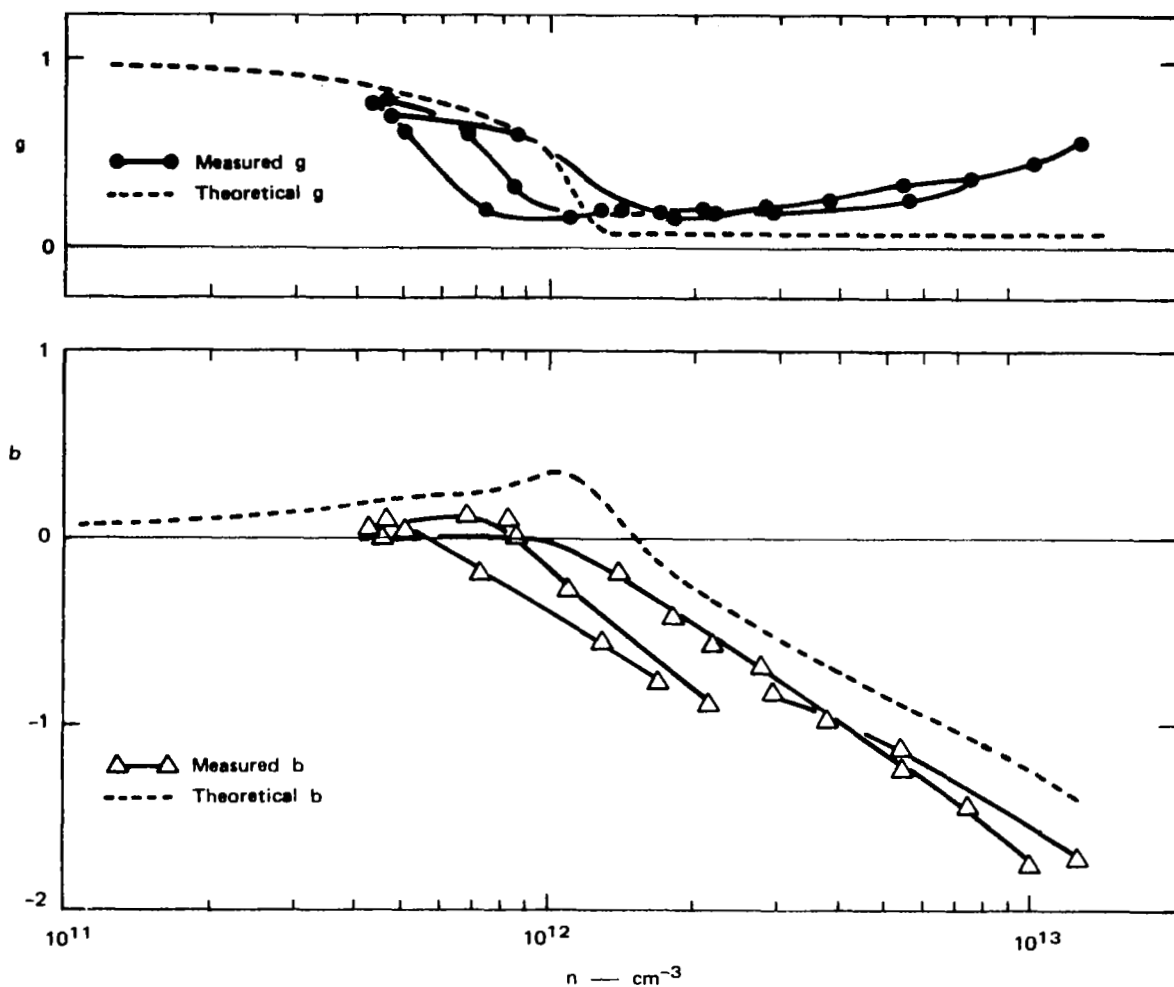
FIGURE 12   COMPARISON OF MEASURED RAM C X-BAND APERTURE ADMITTANCE
WITH THEORY—0.1 torr

TA-7729-26

21

3. 1.0-Torr Measurement Results

Figure 13 shows the pertinent data collected on a 1.0-torr shot. Only the reflection coefficient of the X-band antenna was measured for the 1.0-torr shots. The S-band microwave probes were located electrically as for Figure 7. These data show one example of various "anomalies" that seemed to happen more on the 1.0-torr shots than on the low-pressure ones: the dip in X-band reflection coefficient at about 150 μs after the front is not accompanied by a corresponding dip in the probe current, which rises monotonically in time during the first 250 μs of the test. Such anomalies seem to be the cause of the large scatter in the 1.0-torr data compared with the lower-pressure shots, as illustrated below. One would expect the typical steep slopes of the X-band and S-band reflection coefficients near the critical value to be separated by an order of magnitude. Figure 13 shows that they are separated by only a factor of 2 or 3. For instance, at a point 180 μs from the arrival of the shock, where the inferred electron density is only 3.5×10^{11}, $|\Gamma|_x = 0.58$ and $|\Gamma|_s = 0.65$.

Figure 14 shows both S- and X-band reflection-coefficient data from the 1-torr shots, compared with thoretical predictions of Croswell. It is noted that up to $|\Gamma| \approx 0.6$, the theoretical curves are a fair fit if they are translated in electron density in opposite directions--i.e., if the S-band curve is moved a factor of 1.7 _higher_ and if the X-band curve is moved a factor of 2 _lower_ than predictions. Most of the measured points fall within a factor of two of the translated curve in each case up to $|\Gamma| \approx 0.6$.

$V_p/V_i = 1 \longrightarrow$

$V_p/V_i = 1 \longrightarrow$

$V_p/V_i = 1 \longrightarrow$

ION PROBE NO. 1

ION PROBE NO. 2

$|\Gamma|$

1.0
0.8
0.6
0.4
0.2
0

t_1

t_3

t_2

S-BAND
PROBE NO. 1

S-BAND
PROBE NO. 2

S-BAND
PROBE NO. 3

t_1 SHOCK FRONT ARRIVES
OVER S-BAND APERTURE

t_2 SHOCK FRONT ARRIVES
OVER X-BAND APERTURE

t_3 SHOCK FRONT ARRIVES
AT ION PROBES

$\longrightarrow |50\,\mu s| \longleftarrow$

TIME $\longrightarrow$
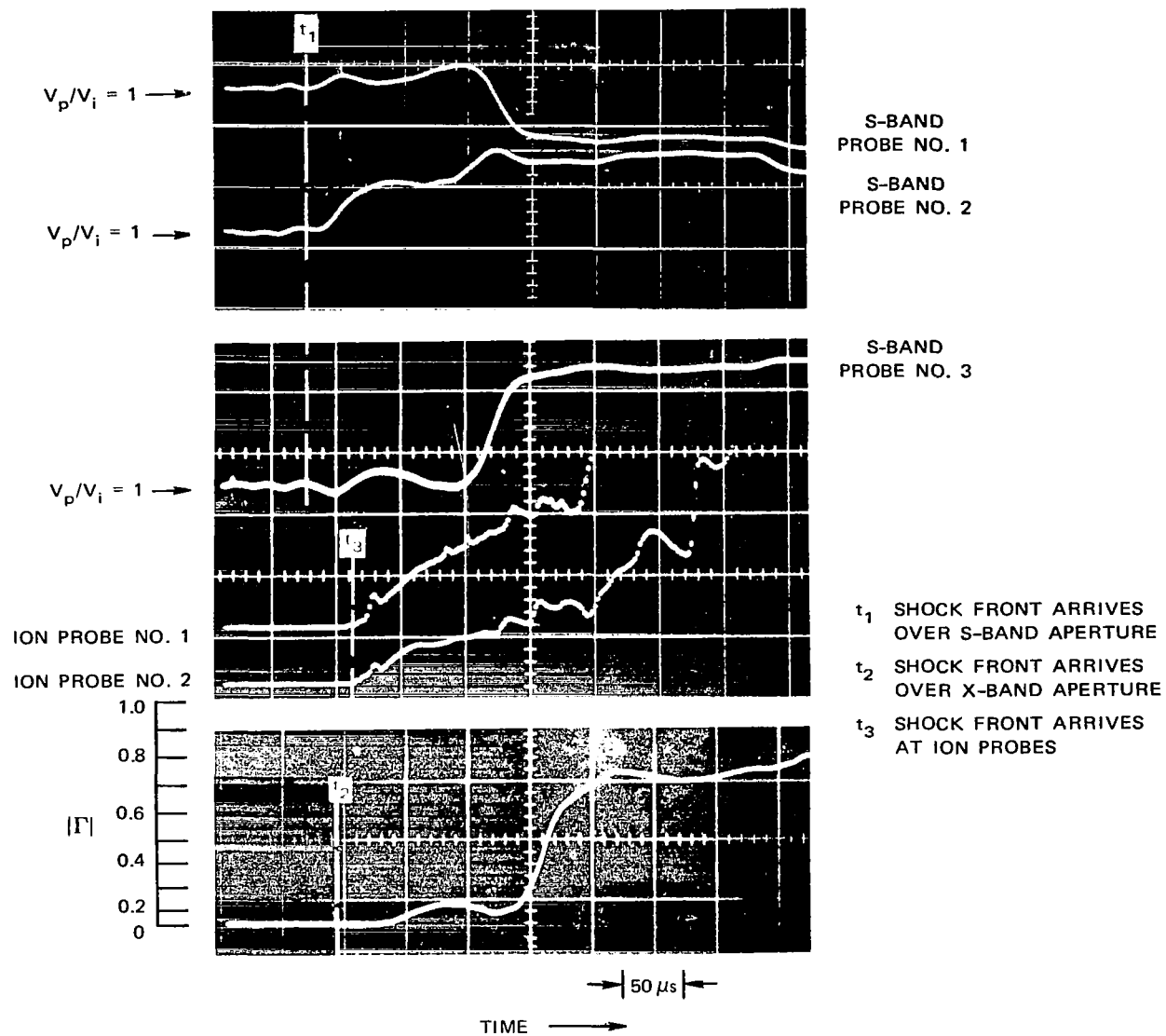
TA-7729-19

FIGURE 13   EXAMPLE OF 1.0-torr SHOT DATA ON RAM C ANTENNAS

23
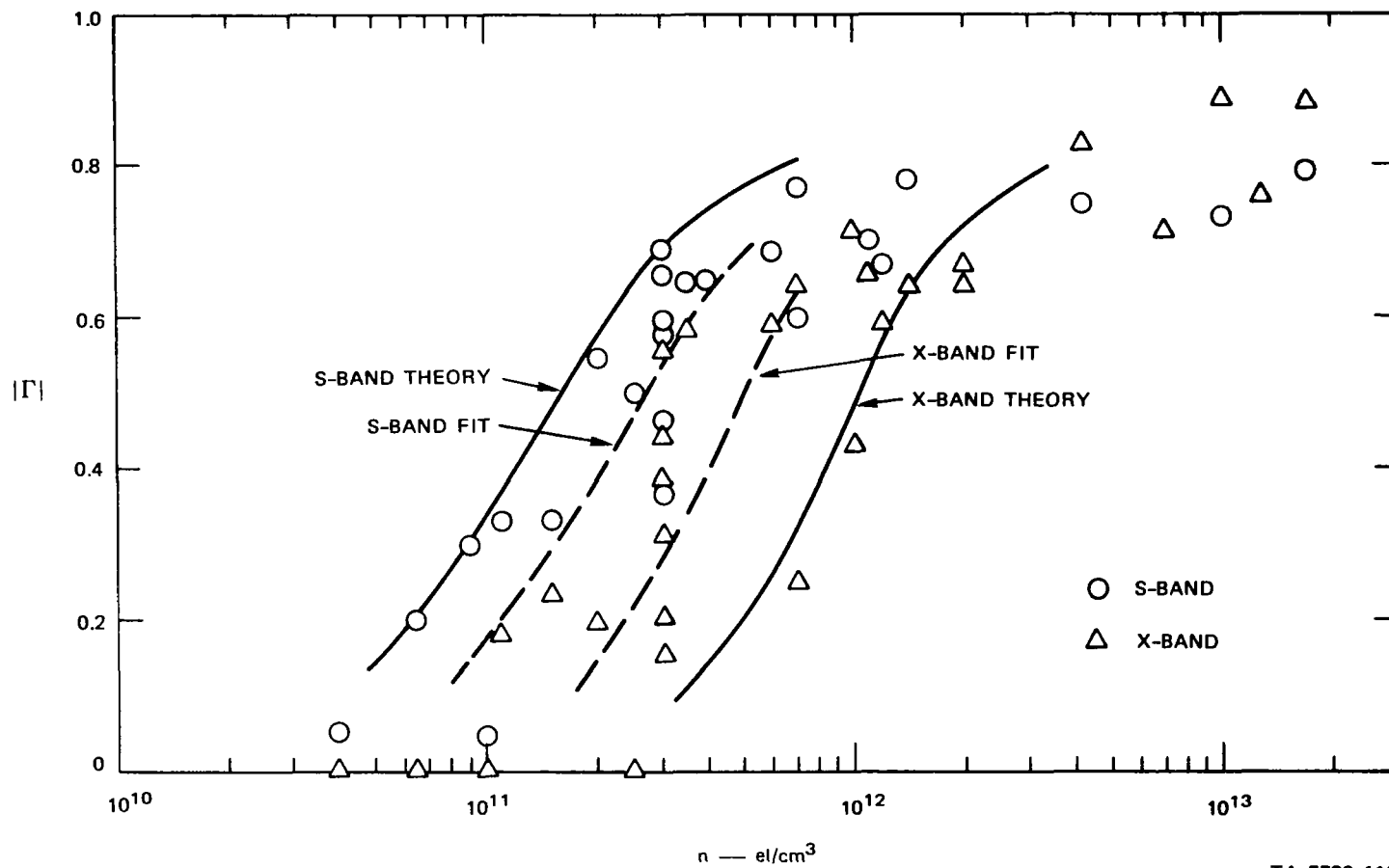
FIGURE 14   RAM C REFLECTION COEFFICIENT DATA AS A FUNCTION OF ELECTRON DENSITY, COMPARED WITH THEORY—1.0 torr

TA-7729-11R

24

It is suspected that the problem of larger scatter in the 1.0-torr data than in the low-pressure shots was caused to some extent by less homogeneous plasmas (transverse to the flow direction). Since the fiberglass tube was required to be qualified by preliminary tests only for the less stringent low-pressure shots, where the mean free path is greater than the scale of roughness of the surfaces, this tube may have contributed much of the problem by giving rise to secondary wave structure in the plasma. This explanation helps in understanding only the scatter in the data, but has no bearing on why the response of the two antennas in terms of electron density is not as far apart (essentially one order of magnitude) as in the case of both the 0.1-torr measurements and theory.

C. RAM C-C Results

The RAM C-C (S-band) antenna had a VSWR of 1.60 in bench measurements and 1.68 when installed in the shock tube, compared with the theoretical prediction of 2.0. Since no conducting walls of this antenna extend through the 0.32-inch-thick Teflon ground-plane cover, it was expected that significant radiation may occur off the edge of the ground plane under any conditions, and especially when the plasma is overdense. A metal foil reflector with the same lateral extent as the plasma was used to simulate the limiting case of $n \to \infty$. This gave $|\Gamma| = 0.84$. Since the flight configuration is completely enveloped by plasma, this indicates that the experiments in the shock tube with the limited ground plane would fail to duplicate the flight configuration by this extent in terms of voltage-reflection coefficient. As will be seen below, the maximum value of $|\Gamma|$ measured with plasma was 0.78, corresponding to the maximum value of n, which was 10^{13}.

Figure 15 shows the measured values of aperture admittance for $p_1 = 0.1$ torr, covering the range from just below critical to two orders

1.1×10^{11}

10^{12}

10^{13}

∞

$n = 0$

With Foil Short
(size of plasma)
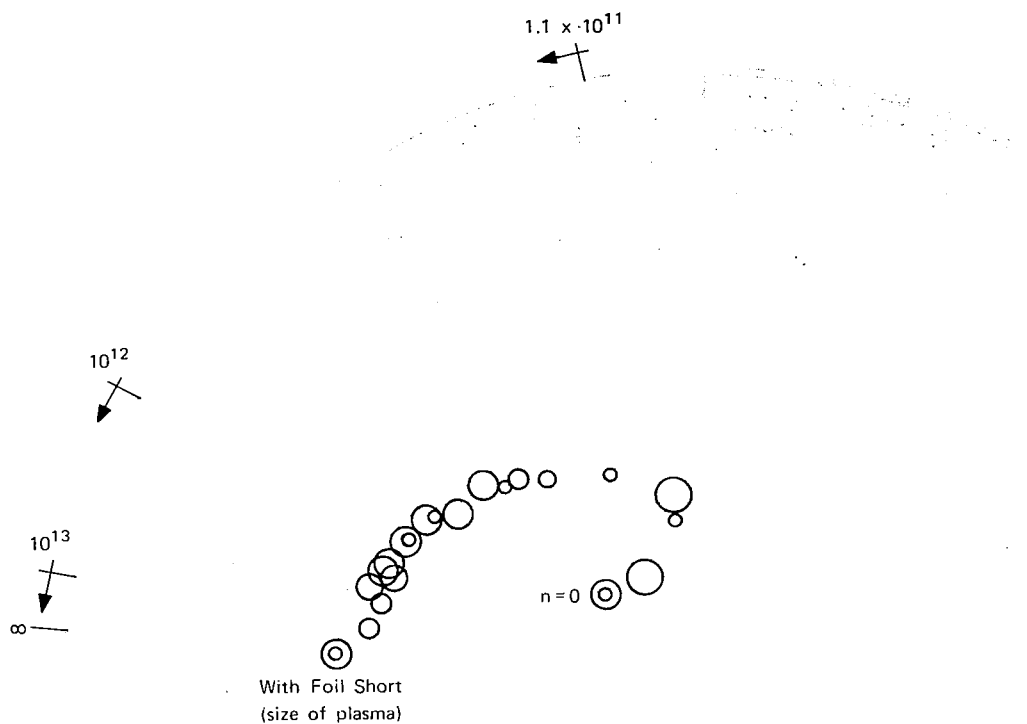
TB-7729-10

FIGURE 15   MEASURED ADMITTANCE OF RAM C-C ANTENNA (p_1 = 0.1 torr), REFERENCED
TO APERTURE

26

of magnitude above.[*] These values are not corrected for line loss.
Figure 16 shows the corresponding reflection-coefficient values, except
that they are corrected for line loss. Also shown are additional data
from two other pressure conditions. It is seen that the 1.0-torr data
show considerably more scatter than the 0.1-torr data, just as for the
RAM C data. Also shown in Figure 16 are predictions for this antenna
by Croswell and Swift reduced by 16 percent to form an approximate
theory appropriate to the experimental configuration, where the maximum
possible $|\Gamma|$ is 0.84. Even with this reduction, the agreement is not
very good, although the location of the maximum slopes of the curves is
at essentially the same electron density.

In the range $(\omega_p/\omega)^2 \gtrsim 1$, the magnitude of the reflection coefficient
is largely determined by the aperture conductance, which is sensitive to
the limited lateral extent of the plasma. This antenna was also designed
for determining electron density above critical mainly by the dependence
of the susceptance on n in this region. Figure 17 shows the measured
susceptance plotted against n. Figure 17 appears to confirm that the
susceptance is an accurate measure of electron density in the two-order-
of-magnitude range above critical. It is seen in Figures 16 and 17 that
several points, actually representing a continuum of data, were derivable
from each of four shots. For each shot, the slope of the lines inter-
connecting the points is virtually identical with the theoretical curve.

---

[*] The phase relationship between the terminal admittance and aperture
admittance was 0.19 guide wavelengths for this antenna.
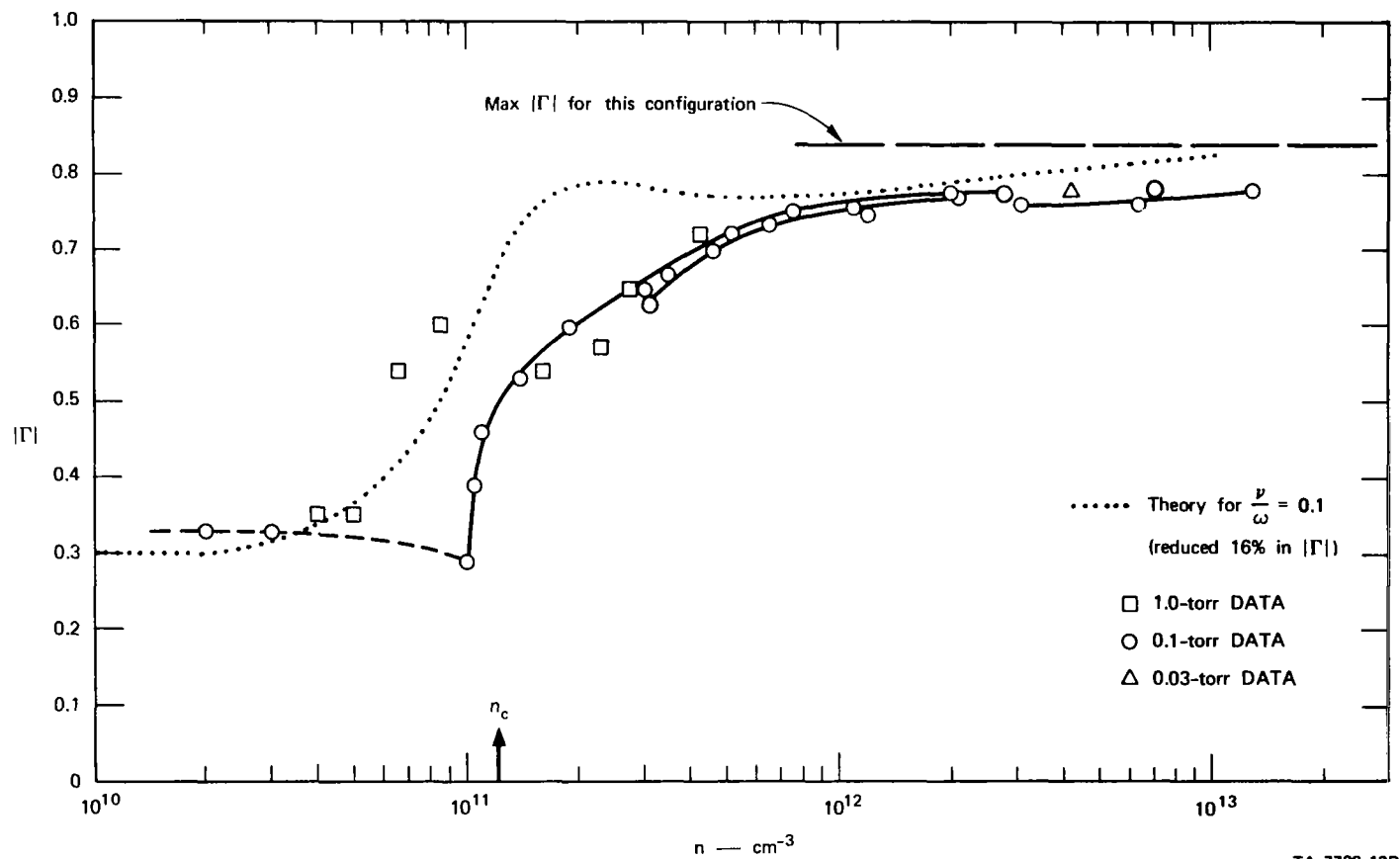
FIGURE 16   REFLECTION COEFFICIENT OF RAM C-C ANTENNA AS A FUNCTION OF ELECTRON DENSITY, COMPARED WITH THEORY

TA-7729-12R
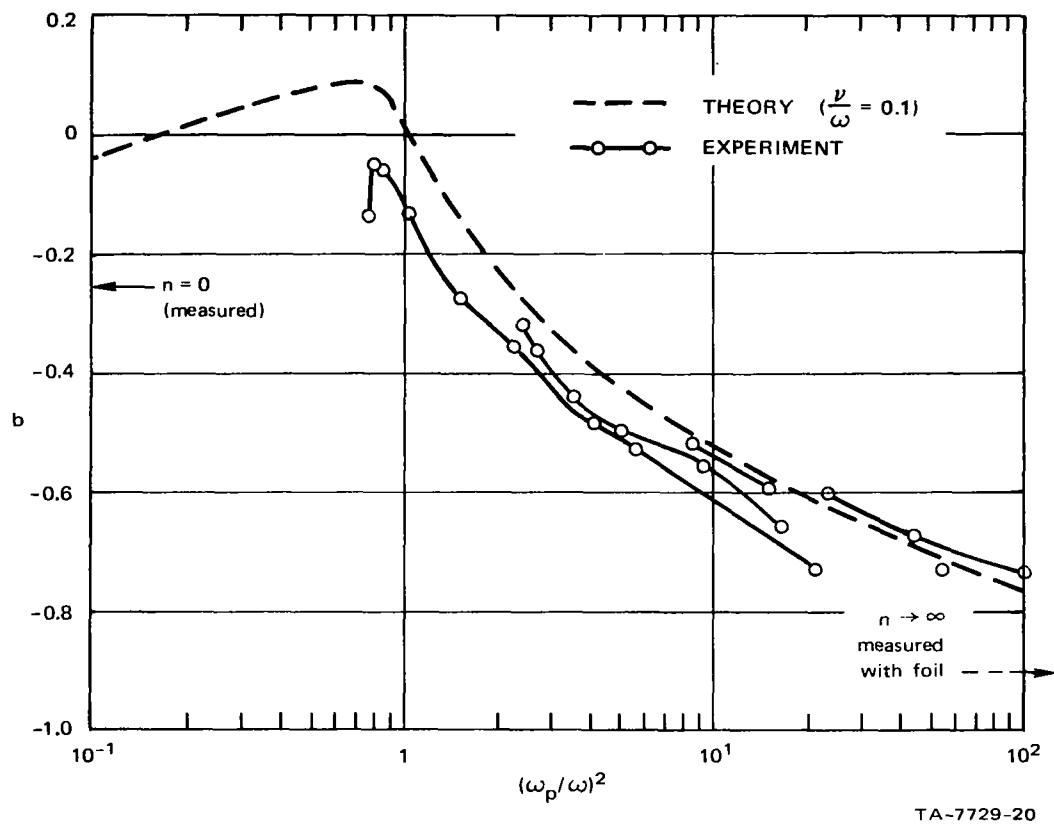
FIGURE 17   APERTURE SUSCEPTANCE, RAM C-C, THEORY VERSUS
EXPERIMENT—0.1 torr

TA-7729-20

29

III   DISCUSSION OF ADMITTANCE MEASUREMENTS FOR PLASMA DIAGNOSTICS

It is felt that the experimental data of Sec. II indicate a confirmation of the methods of Croswell et al.[6] for calculating aperture admittances in the presence of plasma. It was demonstrated how sensitive the conductance is to the configuration used in the measurements, since experimental variation from the theoretical model results in significant discrepancy in the measured conductance. However, this appears not to be the case in susceptance measurements.

Although some experimental data are available, a more complete set is available from theoretical calculations. These calculations can be used to analyze the diagnostics possibilities in aperture-antenna admittance measurements. The most obvious use of antenna admittance for diagnostics is the use of the large changes that usually occur near the critical density--e.g., the sharp increase in $|\Gamma|$ shown in Figure 9. However, this gives a limited range of inferred n, and it is of interest to determine if a larger range can be learned from admittance measurements. Since the admittance is relatively insensitive to n much below critical, this extended range has to be sought above critical. And, indeed, it appears that the first two or three orders of magnitude in n above critical can be determined from careful measurements of susceptance, as indicated by Figure 17.

However, the point should be made that auxiliary information is actually needed to use measured admittance for inferring electron density during reentry. There are only two pieces of information in the complex admittance measurement, yet one needs to determine not only the collision frequency and peak electron density, but also the profile in n. Just

what auxiliary information is used depends upon various confidence levels. For instance, if the profile is being measured during flight by Langmuir probes, as was the case in RAM C-1 and RAM C-2, then this would probably be used in preference to theoretical predictions. Then g and b could be used to determine collision frequency and the absolute level of the probe-measured profile in n.

An example of the importance of the profile determination can be made by an analysis of the dependence of phase of the reflection coefficient (which is essentially determined by b in the overcritical region) upon the scale of the profile and upon peak n, as determined from theoretical calculations. Figure 18 shows two parameters, δ_{pk} and n_{pk}, each of which can be varied when the other is kept constant, using a parabolic boundary layer profile in n. Figure 19 shows that the phase will vary almost the same way when n_{pk} is varied as when δ_{pk} is varied, provided d_c, the distance out to the critical density contour, is the controlling parameter in each case. It also shows there is little difference in phase between a plane wave and circular or rectangular apertures. Figure 18 gives an indication of why d_c is the approximate controlling parameter. Showing attenuation as a function of distance for the case when $n_{pk} = 3 \, n_c$, it indicates that the fields penetrate very little beyond this point.

Figure 19 shows that a narrowing profile cannot be distinguished by a phase measurement from an increasing n_{pk}. Since these two changes are known to occur simultaneously during reentry (prior to significant slowdown), it is clear that auxiliary information is needed in some form to infer n with confidence.
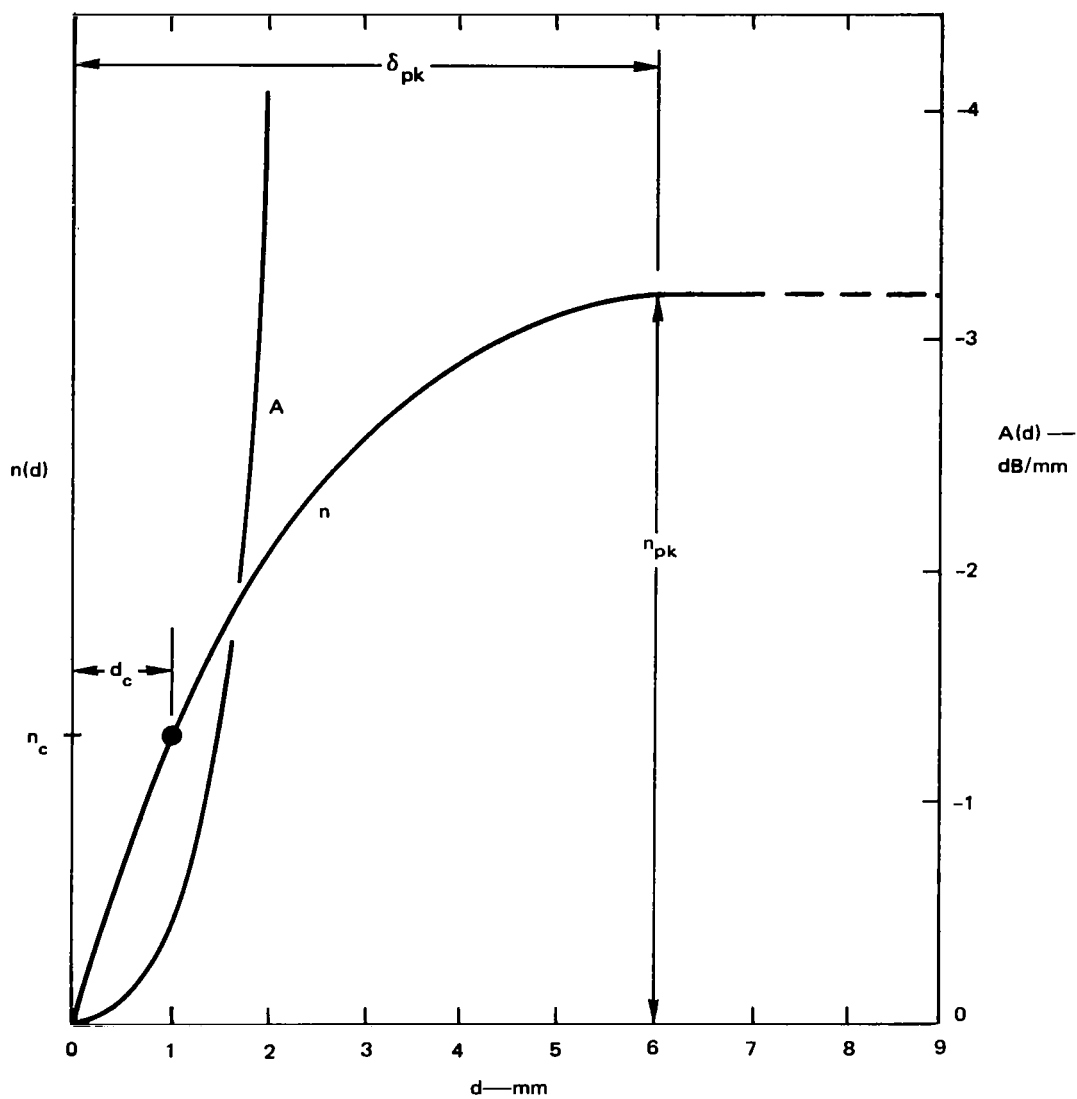
FIGURE 18   INVERTED PARABOLIC PROFILE OF ELECTRON DENSITY AND
CORRESPONDING SPECIFIC ATTENUATION (one way) FOR CASE
SHOWN WITH $\nu/\omega = 0.4$, $f = 10^{10}$ Hz (Rectangular Aperture)
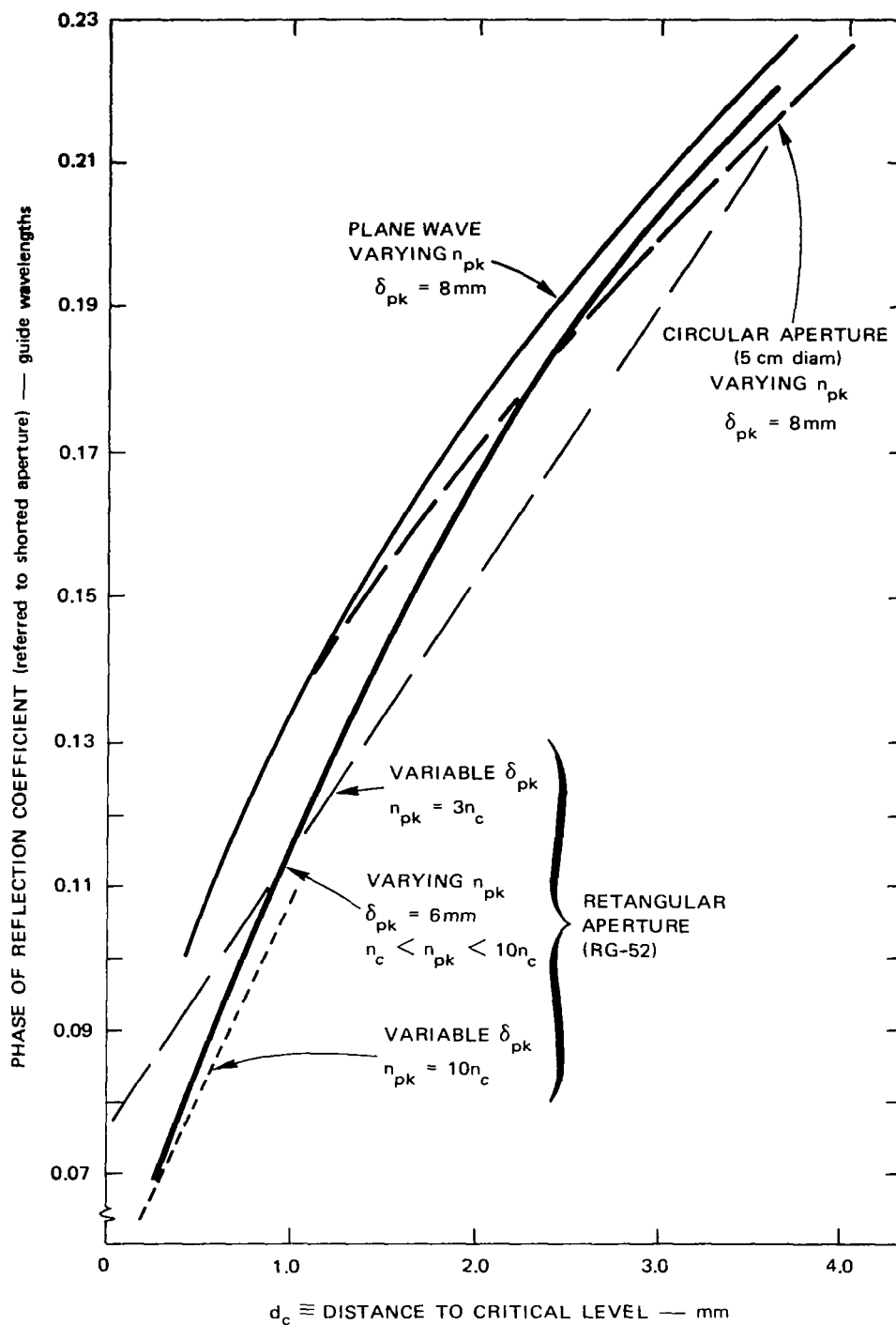
FIGURE 19   COMPARISON OF THEORETICAL REFLECTED PHASE VARIATION
WITH d_c FOR DIFFERENT SCHEMES OF VARYING d_c AND
DIFFERENT APERTURES ($f = 10^{10}$ Hz, $\nu/\omega = 0.4$)

IV MEASUREMENT OF EFFECTS OF INJECTING SF_6 ON IONIZATION

A. Background

The reduction of electron density in the flow-field of reentry ve-
hicles would be helpful in improving communications, reducing radar cross
section, and raising the thresholds for voltage breakdown of antennas.
One means for accomplishing this reduction is by addition of electrophilic
chemicals to the flowing gases. Unfortunately, some of the most effec-
tive chemicals at room temperatures, such as SF_6, dissociate rapidly at
temperatures where the problems of blackout and antenna breakdown are
worst (i.e., above $3000°K$). Thus, it was decided to add the chemical
locally just upstream of an antenna to take advantage, if possible, of
the period before the chemical gets thoroughly heated by the hot air.
Earlier measurements at SRI using SF_6 pre-mixed with the air in the shock
tube showed little difference from the same measurements in air, with
regard to both thermal and RF ionization.

B. Mechanisms for Alleviation

The condition under which chemical alleviation of high plasma density
is most easily achieved is when the electron density for some reason is
higher than the locally existing source(s) of ionization would warrant.
A common example of this is in an expansion region of flowing ionized
gas, where cooling occurs but electron-ion recombination is not fast
enough to reduce the electron density to the value that would exist if
the local thermal ionization rate were in equilibrium with the losses.
A similar situation exists when a sample of gas, having been ionized by
exposure to strong RF electric fields as it flows over an antenna aperture,

is swept beyond the region of high field strength. In either case, the attachment of the electrophilic molecules can be very effective since the rate of production of new electrons may be quite low or nonexistent. However, in most cases where plasma alleviation is required, the injectant must work in an equilibrium or near-equilibrium situation where the ionization source is strong.

There is an important difference between thermal ionization rates and RF-induced ionization rates. Since thermal ionization in air is a result of neutral-neutral collisions, it is independent of the electron density. RF-induced ionization results from electron impact on neutrals; hence the rate is proportional to the electron density itself, causing the cascading effect called "breakdown."

The mechanisms for plasma alleviation by chemicals can be visualized in the framework of the electron continuity equation, which is constructed by equating the electron production rates with electron loss rates. Consider first the steady-state situation with only thermal ionization at a rate S (electrons per cm^3 per second) countered by recombination and attachment. This gives

$$S = \alpha n^2 + \nu_a n \tag{1}$$

where α is the recombination coefficient (cm^3/s) and ν_a is the attachment rate (ionizations/s). The equilibrium density for this situation (assuming conditions uniform enough to ignore diffusion losses) is derived by solving Eq. (1) for n, giving

$$n = \frac{1}{2}\left[\left(\frac{\nu_a}{\alpha}\right)^2 + \frac{4S}{\alpha}\right]^{1/2} - \frac{\nu_a}{2\alpha} \quad . \tag{2}$$

1. Thermal Plasma Alleviation

Alleviation of thermal ionization is generally achieved in two ways. One is directly through attachment in equilibrium conditions, as represented by Eq. (2). Figure 20 shows equilibrium n as a function of attachment rate for four different values of S and for the value of α inferred from the rise-time measurements reported in Ref. 3. Two values of S correspond, for $\nu_a \approx 0$, to $n_{equil.} = 10^{11}$ (as would be approximately the case for a shock speed, u_s, of 3.25 mm/μs in air at 1 torr), and two correspond to $n_{equil.} = 10^{12}$ (as for $u_s = 4.0$ mm/μs), for $\nu_a = 0$. Two values of S (1.3×10^{17} and 7×10^{13}) were generated by including a small diffusion loss rate in addition to recombination in the region where $\nu_a < 10^4$. It is seen in Figure 20 how greater attachment rates are required to reduce n to 10^{10} at gas temperatures of 3920°K. Since the electrophilic molecules undergo thermal decomposition faster at higher temperatures (and the daughter products have lower attachment rates than the parent), alleviation at high temperatures requires a much higher mole fraction of the chemical to be as effective as at lower temperatures. Modica[6] calculated that 7 μs after shock heating to 3820°K (at a pressure of 5.42 atmospheres), the concentration of SF_6 is reduced by three orders of magnitude, with most of it already completely dissociated to atomic fluorine and sulfur.

The second mechanism for achieving thermal plasma alleviation is through cooling by mass addition. If recombination following the cooling is slow, electrophilic action would be very effective in reducing the density to the equilibrium value. It appears feasible to use SF_6 to alleviate the thermal-plasma problem in nonequilibrium flow around lifting vehicles for some distance into the atmosphere, perhaps down to 200 kft.
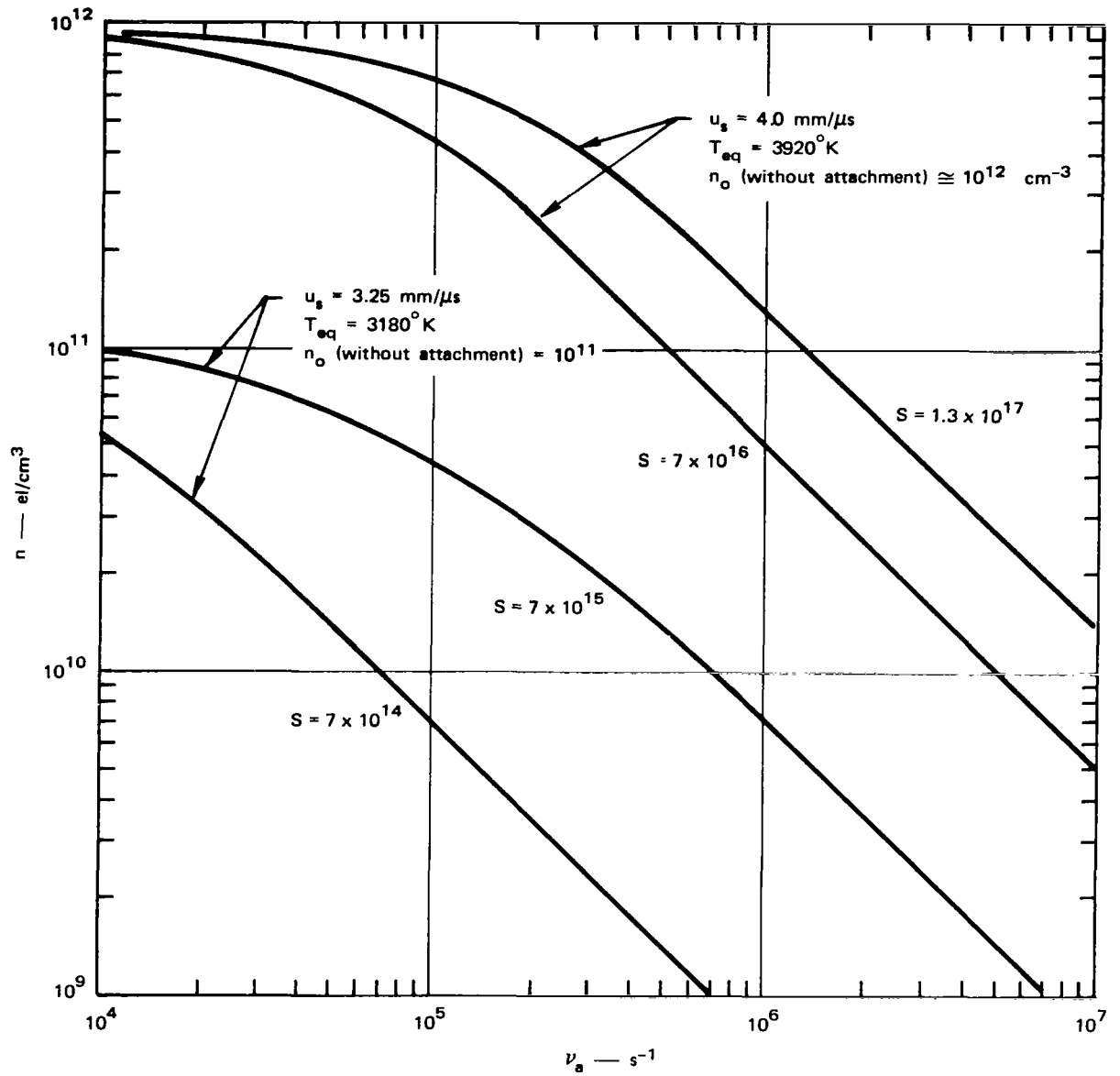
TA-7729-13

FIGURE 20   EQUILIBRIUM ELECTRON DENSITY AS A FUNCTION OF ATTACHMENT
RATE FOR FOUR VALUES OF THERMAL IONIZATION RATE, S

2. RF Ionization Mechanisms

Consider the production of electrons at a rate $\nu_i n$, where ν_i is the RF ionization rate, opposed by an attachment rate $\nu_a n$. The continuity equation is written

$$\frac{\partial n}{\partial t} = \nu_i n - \nu_a n \tag{3}$$

for which a solution is

$$n = n_0 e^{(\nu_i - \nu_a)t} \tag{4}$$

where n_0 is the electron density at $t = 0$. ("Breakdown" is said to occur when n grows to n_c, the critical density.) Since in this case both ionization and attachment rates are proportional to n, the attachment rate subtracts directly from the ionization rate. If ν_a is made as large as ν_i, the RF ionization is completely and directly negated.

There are other ways to increase losses of electrons formed by RF ionization. If the thermal electron density, n_0, is high enough that space-charge effects inhibit electron diffusion to regions of low density, the phenomenon is called ambipolar diffusion. If diffusion losses are included in Eq. (3), with simple boundary conditions applied, such as parallel plates, then solutions are written with ν_i diminished by subtracting not only ν_a but also D/Λ^2, where D is called the diffusion coefficient and Λ is the characteristic diffusion length. The applicable diffusion coefficient in air for ambipolar diffusion is reduced by a factor of about 100 compared with the no-space-charge-effects case of ("free") diffusion. Thus, if an electrophilic injectant reduces the

39

n_0 flowing over an antenna to free-diffusion levels, alleviation is achieved to some extent. Because the diffusion coefficient varies inversely as the gas density, ρ, diffusion is an important loss mechanism at relatively high altitudes, generally down to where $\nu \approx \omega$. Around blunt vehicles reentering at ICBM speeds, n_o reaches ambipolar levels (typically 10^6 or 10^7) well above the altitude where $\nu \approx \omega$. Since the factor of 100 in D translates to a power-threshold difference of approximately 6 dB in the high-altitude regime, the maintenance of n_0 at free-diffusion levels over an antenna aperture offers a significant potential for breakdown alleviation at high altitudes.

Since diffusion is most effective at high altitudes and attachment is most effective at low altitudes, the breakdown power threshold as a function of altitude possesses a minimum, occurring approximately where $\nu = \omega$. Because of this dependence upon collision frequency, the thresholds can be manipulated somewhat by controlling the collision frequency. On the low-altitude side of the minimum it is desirable to increase ν such as to shift, in effect, to a low altitude where the threshold is higher. This increase in ν can be accomplished by use of an injectant to cool the gas, thus increasing its density, or by using an injectant with larger collision cross section than air. Unfortunately, this effect is deleterious at altitudes higher than the minimum, since it reduces diffusion losses.

Since RF ionization rates in air at a given field strength and pressure are somewhat higher at higher temperatures,[7] cooling of the hot air by an injectant will directly affect breakdown by reducing ν_i.

Figure 21 illustrates two of the above mechanisms. This figure shows the increased thresholds measured earlier in cold homogeneous mixtures of SF_6 and air. From these results it has been inferred that ν_a of the one-percent (by volume) mixture is of the order of $10^8 p$ per
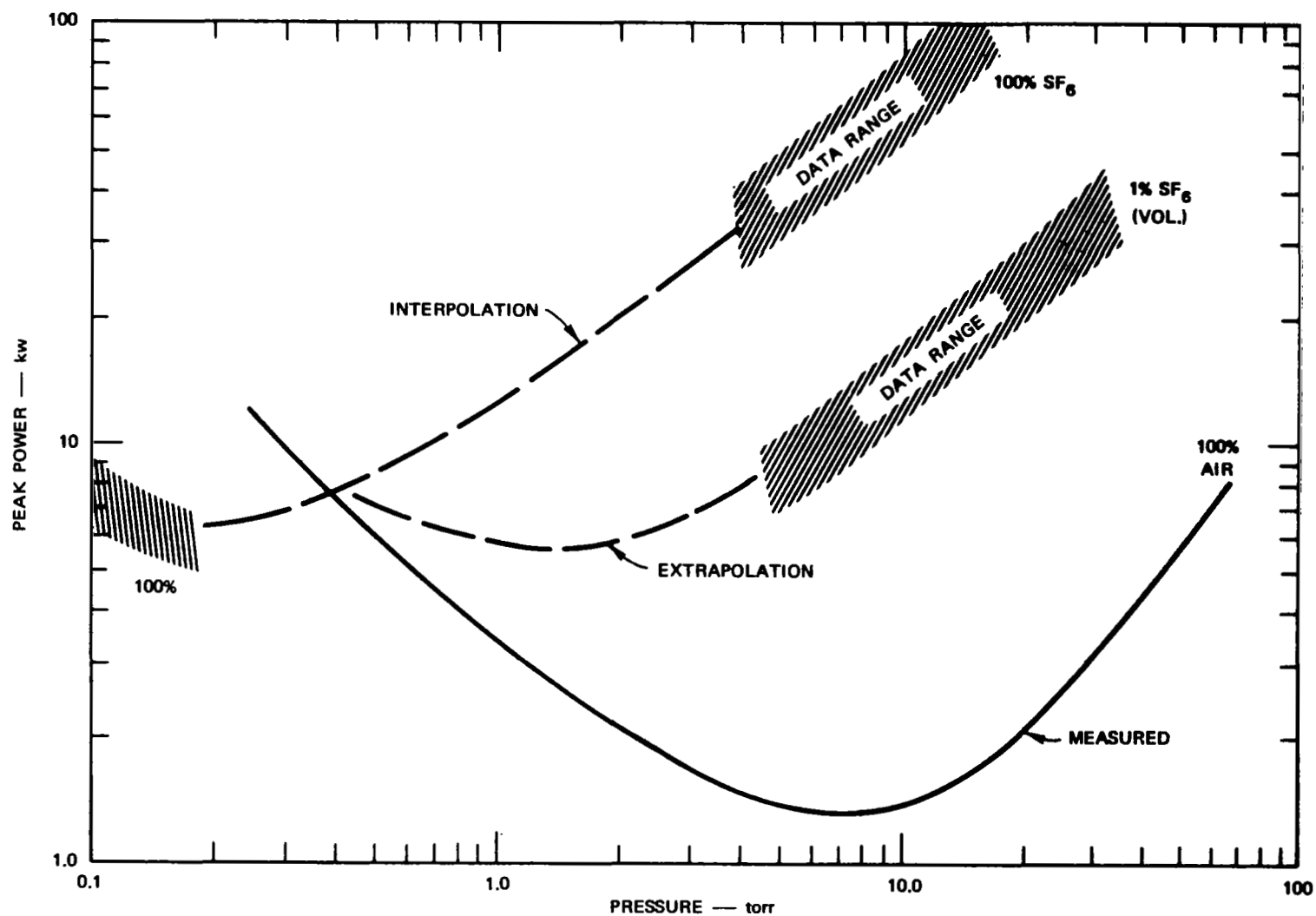
FIGURE 21   BREAKDOWN THRESHOLD FOR X-BAND SLOT IN AIR AND SF₆ (room temperature)

TA-657582-20

second, where p is the total pressure in torr. This rate is about 10^4 times that in air alone, and is quite close to the rate measured by Mahan and Young.[8][*] It appears that the only major difference between the one-percent mixture and the 100-percent SF_6 is in the collision frequency, manifest as a shift in abscissa. The undesirable reduction in threshold at low pressure caused by increased collision frequency is seen on the extreme left-hand side of the 100-percent curve. Since there is no thermal decomposition problem in the case of Figure 21, the attachment rate of $10^8 p$ quite probably represents the upper bound in attachment efficiency that can be achieved in the reentry plasma layer.

C. Experimental Arrangement and Procedure

Figure 22 shows the apparatus used in the shock tube for most of the tests. The X-band slot antenna was plugged by a Teflon block to make a surface flush with the brass plate used as a ground plane. The plate has a sharp leading edge to minimize the effects of intercepting the flow. The SF_6 was injected through a porous plug that was placed flush in the plate about 1/2-inch upstream of the antenna.

It was reported by Thompson[9] that there is an optimum placement of the injection port upstream of an aperture for thermal alleviation effects. Apparently, if the distance is too great, thermal decomposition degrades the effect. But if the distance is too small, the mixing of the injectant may not be complete enough. For the faster shock-tube flow, in the work reported here, it was expected that the depth of

---

[*] It would be expected that Taylor's rates would be lower than those of Mahan and Young because their work was at low electron temperature where the attachment cross section of SF_6 is believed to peak, but Taylor's results are only preliminary.
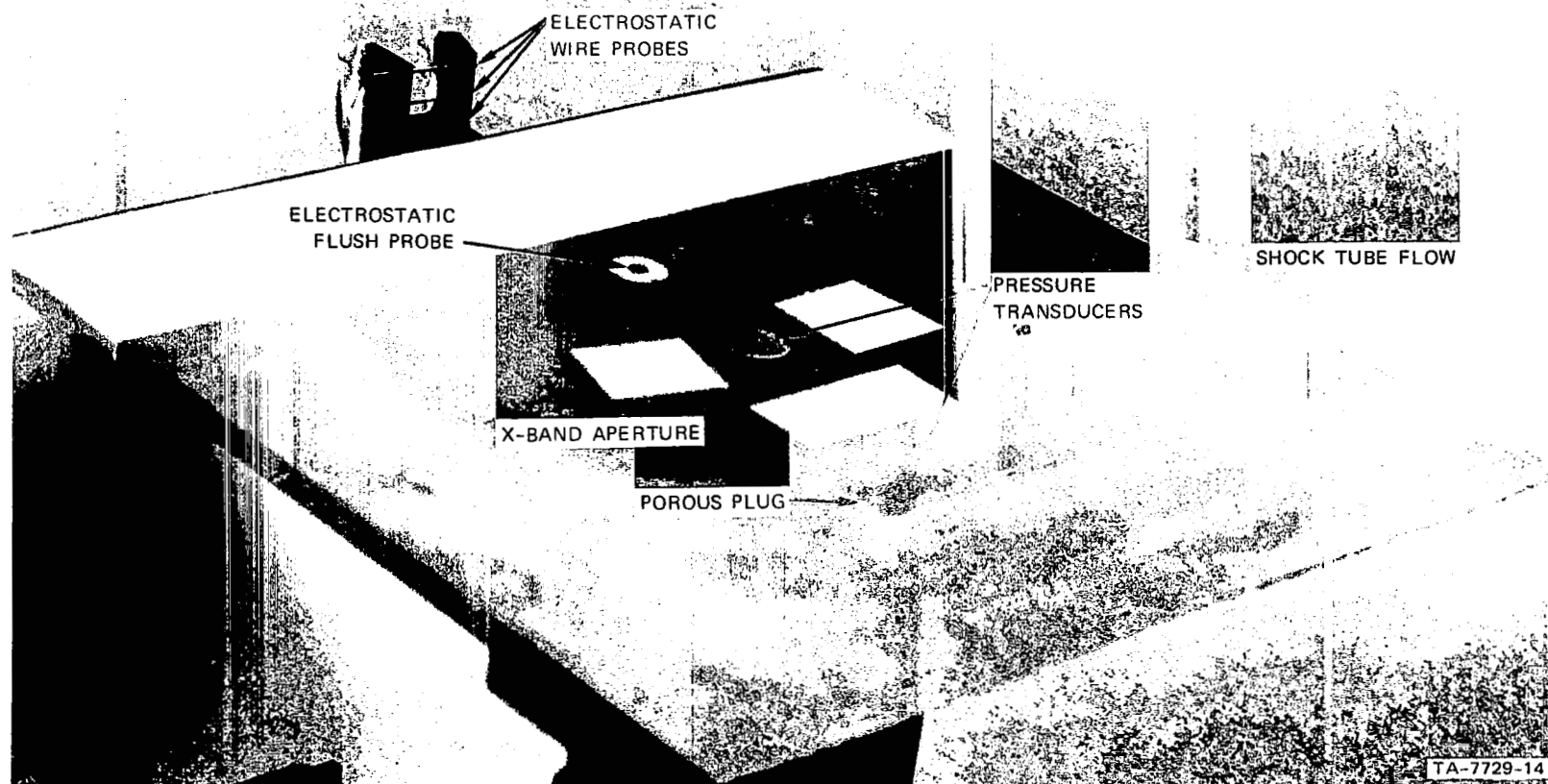
FIGURE 22   PHOTOGRAPH OF ANTENNA, PROBES, AND POROUS PLUG IN PLATE USED IN SF_6 INJECTION MEASUREMENTS

penetration of the injectant would be limited. However, since breakdown occurs in the high field quite near the aperture, it was expected that an effect on the threshold could be discerned for almost any penetration depth. Because the shots were 1 torr initial pressure, wedge probes were used to monitor the ion-density profiles off the plate, but it was decided to replace these by 2-mil-diameter wire probes to get better definition, since the wedges are bulky for the scale of distances involved. Three wire probes were mounted on a wedge-shaped structure, located approximately 30, 60, and 90 mils off the plate at the trailing edge.[*] A flat electrostatic probe was placed flush in the plate for additional diagnostics. Pressure transducers were used in an attempt to determine if there was a measurable difference in pressure on shots when injection was used, but the results were not conclusive.

Since pulsing the injection in times comparable with the shocktube test time ($\sim$100 μs) appeared only marginally feasible at best, it was decided to fire the shock into a steady-state situation with the SF_6 flowing from the plug and being convected downstream by a flow of air established by injecting the air near the driver and pumping rapidly at the dump-tank end. The total flow of air and SF_6 prior to the shot was 0.4 scfm (standard cubic feet per minute—volume referenced to STP conditions). The SF_6 rates were varied from zero to 0.2 scfm from shot to shot. The 1-torr initial tube pressure was chosen (rather than a lower one) to minimize diffusion of the SF_6 toward the driver. As it was, it was estimated that several microseconds of test time would be required to sweep the diffused SF_6 downstream so as to give a flow that

---

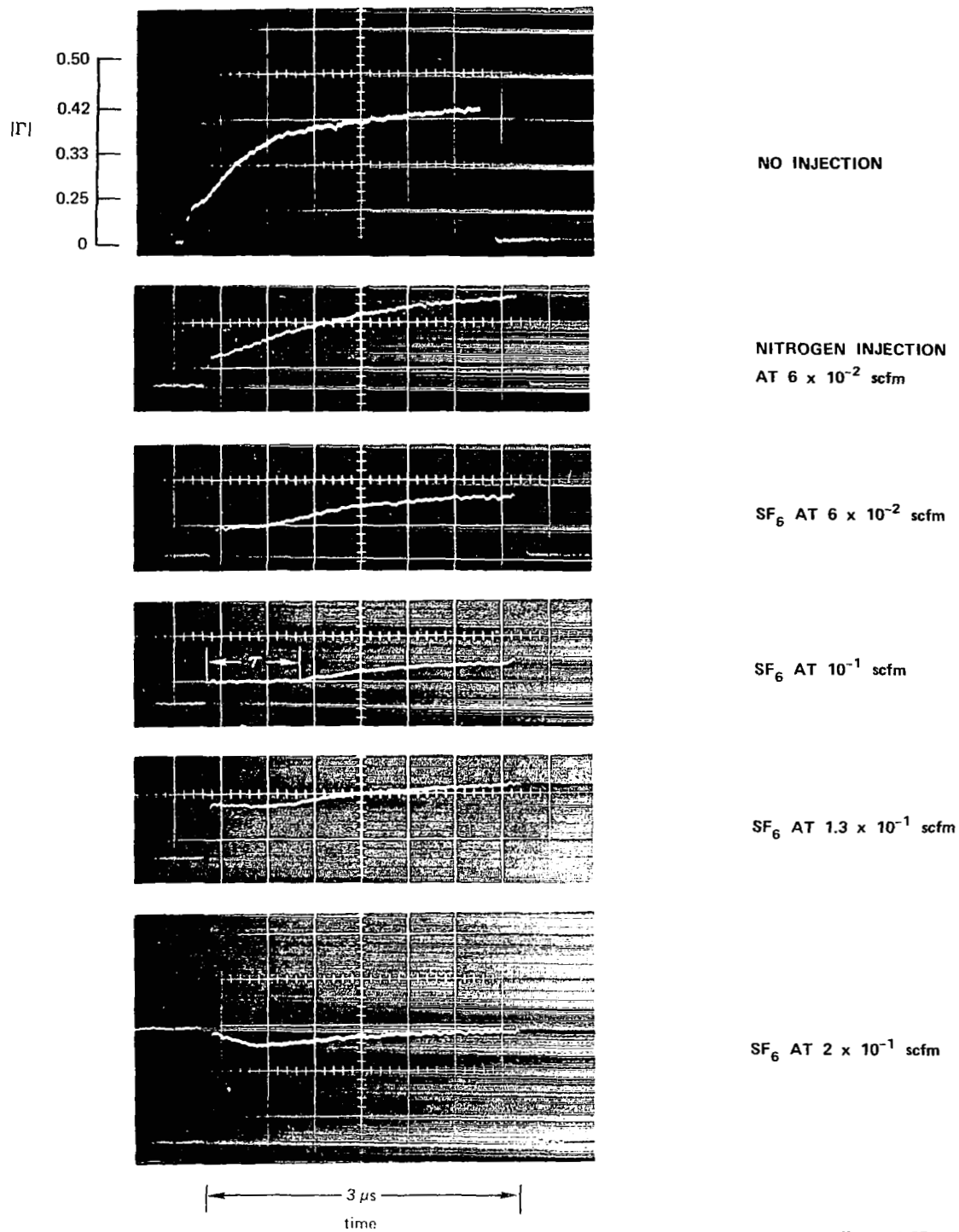[*] The wire spacing shown in Figure 22 was a later alteration that does not apply to the data.

is predominantly (99%) air over the aperture, with SF_6 entering only locally. Another reason for selecting no lower than 1-torr initial pressure is that the breakdown threshold minimum for X-band occurs at approximately these conditions. A shock speed of about 3.25 mm/μs was selected so that the temperatures were low enough (3200°K) to minimize the thermal decomposition of the injectant.

A single microwave pulse 3 μs long was transmitted during the nominal test time while the shocked air was flowing over the antenna, with the reflected pulse displayed to indicate when, during the pulse, the RF-enhanced electron density reached approximately the X-band critical level. The thermally generated electron density in air was about 10^{11} el/cm^3 for a shock speed of 3.25 mm/μs. The sweep of the oscilloscope traces was triggered by an electrostatic probe upstream of the plate, and the microwave pulse was timed by using an appropriately delayed pulse to the magnetron modulator.

D. Results of Measurements

1. RF Ionization

Figure 23 shows a sequence of reflected pulses for six different shots, corresponding to four rates of SF_6 injection compared with injection of N_2 (as a coolant gas), and with no injection. The incident power in each case was 400 W. Reflected pulses are used as an indication of breakdown effects because the reflected signal shows an increase at that time during a pulse when the electron density somewhere over the aperture reaches approximately the critical value. Thus the important parameter is the height of the pulse at any time compared with the

$|\Gamma|$

0.50
0.42
0.33
0.25
0

NO INJECTION

NITROGEN INJECTION
AT 6×10^{-2} scfm

SF_6 AT 6×10^{-2} scfm

SF_6 AT 10^{-1} scfm

SF_6 AT 1.3×10^{-1} scfm

SF_6 AT 2×10^{-1} scfm

$3 \mu s$

time

TA-7729-2R

FIGURE 23 REFLECTED X-BAND PULSES FOR VARIOUS INJECTION SCHEMES,
WITH 400 W INCIDENT POWER

46

initial height.* For example, the fourth pulse $\left(SF_6 \text{ at } 10^{-1} \text{ scfm}\right)$ shows

a clear-cut change in reflection coefficient starting at 1.6 μs. Not

only is this a longer time than the traces above it, but also the re-

flected power does not reach as **high** a level as in the traces above it.

While it appears that in the two lower traces the reflection coefficient

is reduced somewhat more, relative to the initial pulse height, the dip in

the early portion of the pulse is not understood.

The net ionization rates $\left(\nu_i - \nu_a\right)$ can be inferred from the top four

traces in Figure 23 by using Eq. (4), substituting $n = n_c$ at $t = T$, where

T is the time required for n to grow to n_c, as illustrated in the fourth

trace. This gives:

$$\nu_{net} \equiv \nu_i - \nu_a = \frac{\ln(n_c/n_0)}{T} \quad . \tag{5}$$

Table I shows the calculated values of ν_{net} corresponding to the four

top traces in Figure 23, and the values of ν_a for the two SF_6 injection

rates inferred from these values. It is assumed that the decrease in

ionization rates can be attributed to a combination of cooling and

attachment, and that the N_2 case indicates how much is due to cooling

for that rate of injection. Since the increase in reflected power was

miniscule at the two higher rates of SF_6 injection, shots were taken

with incident power of 800 W to determine the effects at this power

level. The data are shown in Figure 24, and the inferred rates are

included in Table I. It appears from Table I that the attachment rates

---

* Only the relative height is important in Figure 23, since the micro-
wave and oscilloscope gains were not maintained at a constant level
from shot to shot. The scale of $|\Gamma|$ on the top trace is accurate
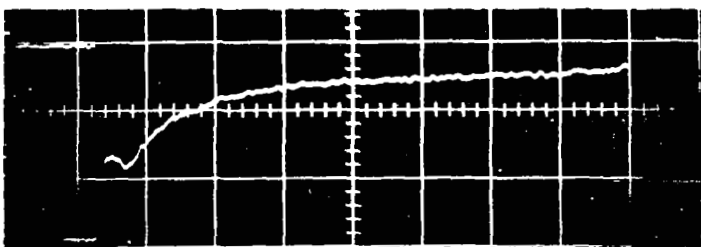only for this trace.
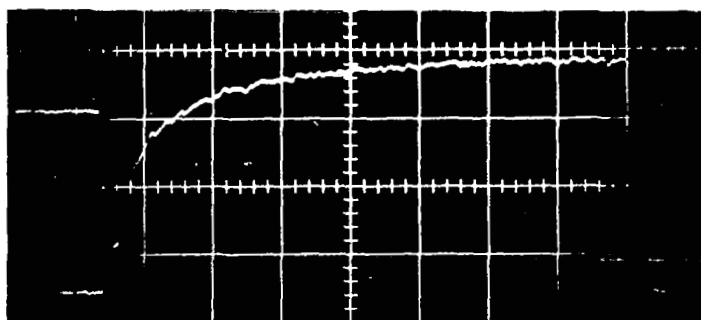
NO INJECTION
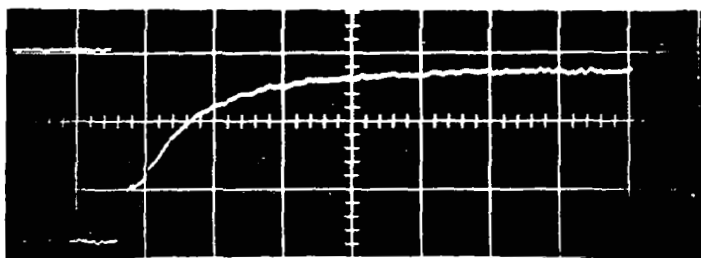
SF_6 AT 6×10^{-2} scfm

SF_6 AT 2×10^{-1} scfm

0.4 μs

TA-7729-23

FIGURE 24   REFLECTED X-BAND PULSES FOR VARIOUS INJECTION
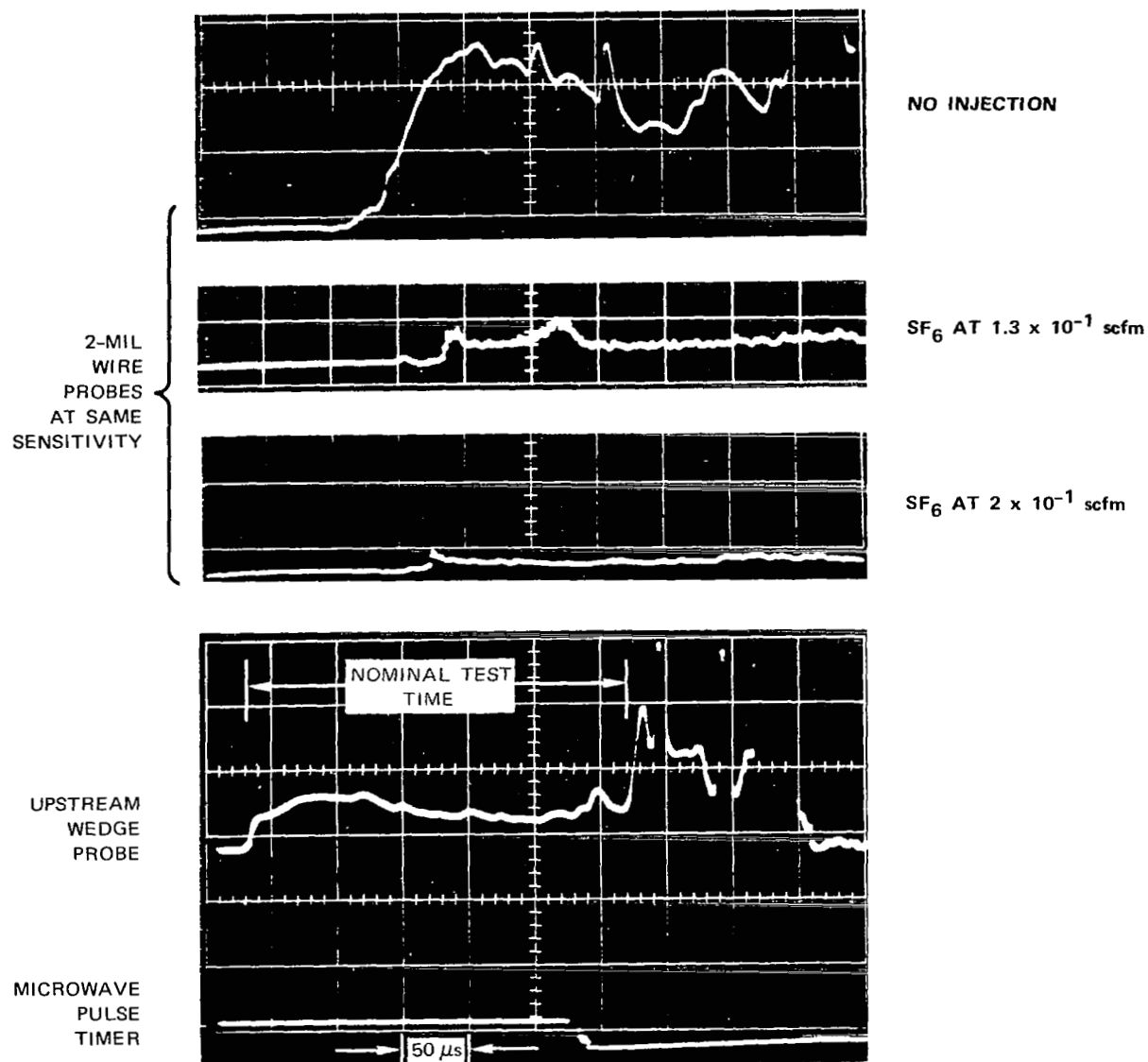SCHEMES, WITH 800 W INCIDENT POWER

Table I

INFERRED IONIZATION AND ATTACHMENT RATES

	400-W Shots		800-W Shots	
	ν_{net}	ν_a	ν_{net}	ν_a
No injection	2.5×10^7	--	5×10^7	--
N_2, 6×10^{-2} scfm	2.0×10^7	--	--	--
SF_6, 6×10^{-2} scfm	5×10^6	1.5×10^7	2.3×10^7	1.7×10^7
SF_6, 10^{-1} scfm	3×10^6	1.7×10^7	--	--
SF_6, 2×10^{-1} scfm	--	--	1.3×10^7	2.7×10^7

achieved by the SF_6 are of the order of 10^7, with less than proportionate increase when the rate of injection is tripled. In terms of pressure, the rate varies from about 1.5×10^6 p to 2.7×10^6 p, since p is equivalent to approximately 10 torr for 1-torr shots. Although the inferred attachment rates are considerably degraded compared with the rate of 10^8 p inferred from cold-gas measurements in Figure 21, they are still significant in terms of threshold reduction. In terms of the hot-air ionization rates of Ref. 7, the improvement is 3 dB for CW attachment-controlled breakdown.

2. Thermal Ionization

Figure 25 shows examples of the ion current gathered by the outermost 2-mil wire probes at the downstream edge of the plate during a shot. Showing data with no injection and two different rates of SF_6 injection, the data show marked reduction in the current. Other pertinent data are given in Figure 25 in the lower traces, showing, for comparison, the current collected by a wedge probe a few centimeters upstream of the

NO INJECTION

2-MIL
WIRE
PROBES
AT SAME
SENSITIVITY

SF_6 AT 1.3×10^{-1} scfm

SF_6 AT 2×10^{-1} scfm

NOMINAL TEST
TIME

UPSTREAM
WEDGE
PROBE

MICROWAVE
PULSE
TIMER

50 μs

TA-7729-24

FIGURE 25   PROBE-CURRENT REDUCTION ON 2-mil WIRE PROBE FOR THREE DIFFERENT
SHOTS (upper three traces), COMPARED WITH WEDGE PROBE CURRENT ON
SIMILAR SHOT SHOWING NOMINAL TEST TIME

50

plate, and, in the lowest trace, the microwave pulse-time monitor on the same time scale. The bias on the wire probes on these shots was -3 volts, a value that brings the ratio of the ion-sheath radius to the probe radius close to that ratio when a -15 volt bias is used with the more familiar 10-mil probes. The electron density inferred from the 2-mil probes with -3 volts bias was within 20 percent of that inferred from a previously calibrated wedge probe on the same shot (without injection). On a given shot, there was negligible difference among the three probes except in the shots with no injection, when the probe nearest the plate collected only one-third to one-half as much current as the other two. Thus it appears that the SF_6 penetrated to at least 0.1 inch off the plate at this location on the plate. The variation of the current with time during the nominal test time on the two upper traces is not understood.

Figure 26 shows a compilation of the results for several shots, including a shot with N_2 as the injectant, where the ion current is normalized to the current without injection. Levels for all three probes are shown in this figure. The same fractional reduction appears to be achieved whether the peak currents (early in shot) or the more-or-less steady values at approximately 250 to 300 μs are plotted. Since the SF_6 attaches electrons, thus forming negative ions, the positive ion current collected by the probes may not be reduced by a factor as great as that by which the electron density is reduced.[10] For example, if there is no ion-ion recombination, the positive-ion density will remain at essentially the initial level, which is the same as the initial electron density. Whether the ion saturation current collected by the probe would be reduced in this case depends upon whether the negative ion current collected by the positive electrode (such as tube walls, etc.) becomes a limiting factor in the probe circuitry. Thus it is
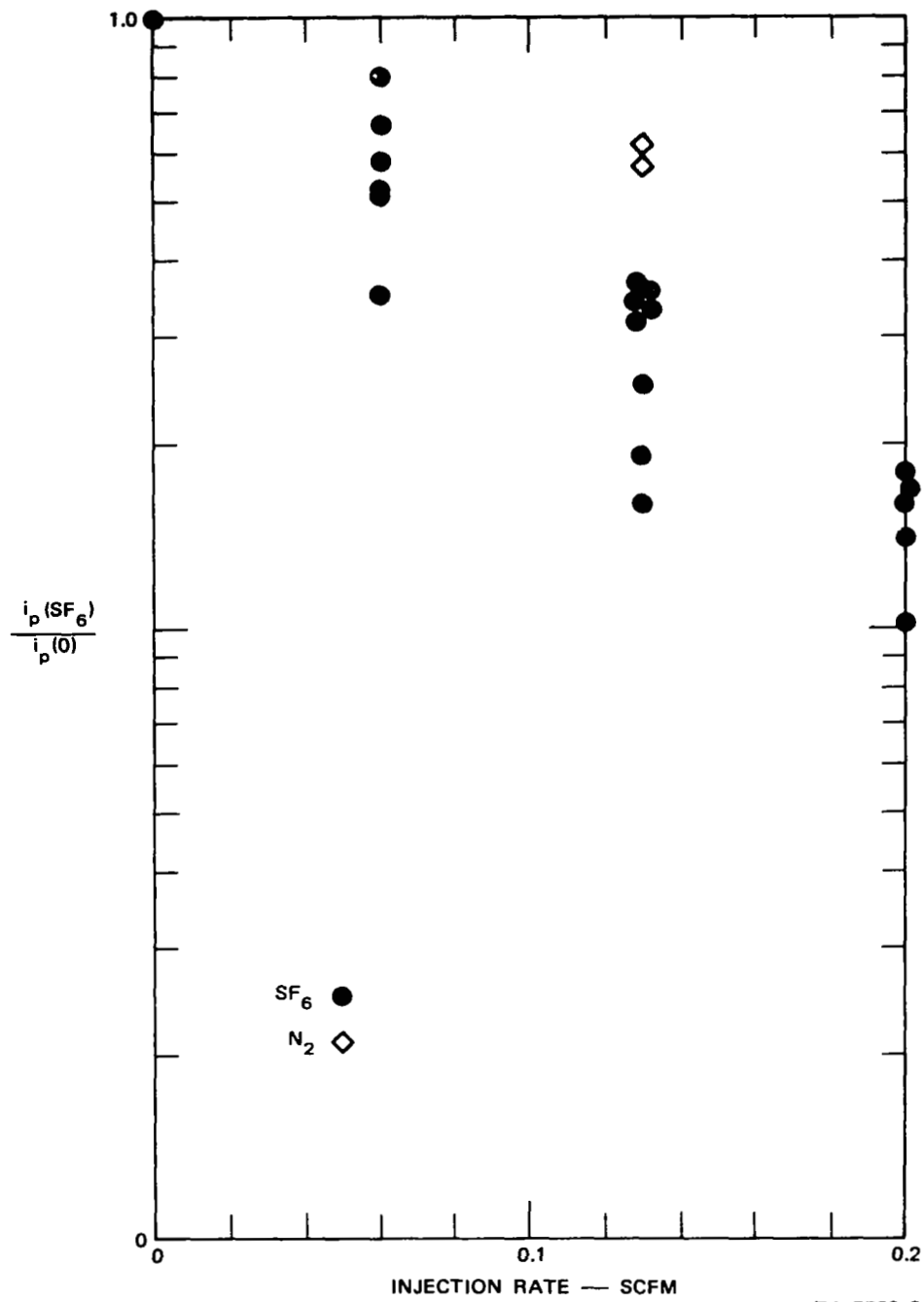
51

FIGURE 26   CURRENT COLLECTED BY 2-mil WIRE PROBES AS FUNCTION
OF INJECTION RATE

possible that the electron density in these tests was reduced by a factor greater than the positive ion currents shown in Figure 26.

E. Discussion and Conclusions

The brief nature of this exploratory study did not allow a determination of optimum location of the injection ports, of optimum injection scheme, etc. The range of rates of injection appeared to be high enough to be effective without being excessive. For example, the flux of the hypersonic air down the shock tube was approximately 60 scfm per square inch of cross-sectional area.

It would be desirable to determine by direct measurement whether the thermal electron density was indeed reduced more than the ion current ratios shown in Figure 26. However, the traces of Figure 23 can be interpreted to indicate that the electron density was not reduced by several orders of magnitude. The important indicator is the initial slope of the reflected pulse when the RF ionization effects are first seen (around $n = n_c$). By evaluating Eqs. (3) and (4) at $n = n_c$, corresponding to $t = \tau$, and eliminating $(\nu_i - \nu_a)$ between them, a relationship between n_o and $(\partial n/\partial t)_{t=\tau}$ is derived:

$$\left(\frac{\partial n}{\partial t}\right)_{t=\tau} = \frac{n_c}{\tau} \, \ell n(n_c/n_o) \quad . \tag{6}$$

Thus for constant n_c and constant τ, the slope at $t = \tau$ depends only on n_o. Although the dependence is weak because of the function ℓn, orders-of-magnitude differences in n_o would be discernible in the slopes

of n vs. t, hence in the slope of the reflected pulses.[*] Thus the lower four traces in Figure 23, which have approximately equal values of τ as required for this comparison, would show increasingly steep initial slopes as the injection rate increases if there were orders-of-magnitude reduction in n_o. For a more thorough study of this type, a measurement, say, with voltage-swept probes or a microwave interferometer, should be used to determine more accurately the reduction in n_o.

It thus appears that a modest alleviation was achieved in these tests with respect to both thermal and RF ionization, and the basic method for exploring the effects was a good one. The thermal ionization reduction of one order of magnitude could be quite significant for situations where the electron density is just above critical. For breakdown threshold effects, it appears that the 3-dB improvement for attachment-controlled breakdown is the best that was obtained at these temperatures, in addition to a modest cooling effect. In this temperature range, and higher, a reduction in n_o to free-diffusion levels does not appear to be feasible unless the configuration, injection scheme, etc. used here were far from optimum. However, it is expected that the situation would improve markedly with small reduction in air temperature[10] due to reduced decomposition of SF_6. Because of this, one could expect to achieve considerable improvement ($\sim$ 6 dB) in diffusion-controlled

---

[*] Although no quantitative studies of this phenomenon have been made, the author has consistently observed the contrast between results such as those shown in Figure 23 and the reflected pulses in cold-gas breakdown, where $n_c/n_{Q} \approx 10^6$ or more. Only the early slopes can be used since the self-quenching attenuation due to the RF ionization begins to take effect and, along with convection effects, causes a "saturation" level of reflected signal.

breakdown (high altitudes) at air temperatures below $3000°K$, but high enough for n_o to be above free-diffusion levels. Such an application might be particularly important in the case of reentry of lifting vehicles, such as the space shuttle, where relatively modest air temperatures are encountered for long periods of time.

REFERENCES

1. W. C. Taylor, "The Effects of a Plasma in the Near-Zone of an Antenna," Final Report, Contract NAS1-3099, SRI Project 4555, Stanford Research Institute, Menlo Park, California (June 1964).

2. W. C. Taylor, "Study of the Effects of a Plasma in the Near-Zone Field of an Antenna," NASA CR-611 (1966).

3. W. C. Taylor, "The Effects of a Plasma in the Near-Zone Field of an Antenna--II," NASA CR-1149 (1968).

4. H. R. Bredfeldt, W. E. Scharfman, H. Guthart, and T. Morita, "The Use of Ion Probes in Re-Entry Physics," Tech. Report 26, Contract SD-103 under ARPA Order 281-62, SRI Project 3857, Stanford Research Institute, Menlo Park, California (May 1965).

5. W. F. Croswell, W. C. Taylor, C. T. Swift, and C. R. Cockrell, "The Input Admittance of a Rectangular Waveguide Fed Aperture Under an Inhomogeneous Plasma: Theory and Experiment," Trans. Ant. and Prop. AP-16, No. 4, pp. 475-484 (July 1968).

6. A. P. Modica, "Microwave Measurements of Nonequilibrium Air Plasmas Behind Shock Waves Containing Electrophilic Gases," J. Phys. Chem. 71, No. 11, pp. 3463-3469 (October 1969).

7. W. C. Taylor, J. B. Chown and T. Morita, "RF Ionization Rates in High Temperature Air," J. Appl. Phys., Vol. 39, No. 1, pp. 191-194 (January 1968).

8. B. H. Mahan and C. E. Young, "Gaseous Thermal Electron Reactions: Attachment to SF_6 and C_7F_{14}," J. Chem. Phys. Vol. 44, No. 5 (March 1966).

9. W. P. Thompson, M. Epstein, and C. J. Lenander, "Microwave Breakdown of the Reentry Boundary Layer," Aerospace Report No. TR-1001 (2240-20)-11, Contract No. AF 04(695)-1001, Aerospace Corporation, El Segundo, California (May 1967).

10. K. E. Starner, "Evaluation of Electron Quench Additives in a Subsonic Air Arc Channel," AIAA Journal, Vol. 7, No. 12, pp. 2357-2358 (December 1969).